The Use of Lidar to Evaluate Existing Incident Managment System on I-80 in Morris, Essex, and Passaic Counties in Northern New Jersey

Project No. 7290
Report No. 980004-7290
July 1998

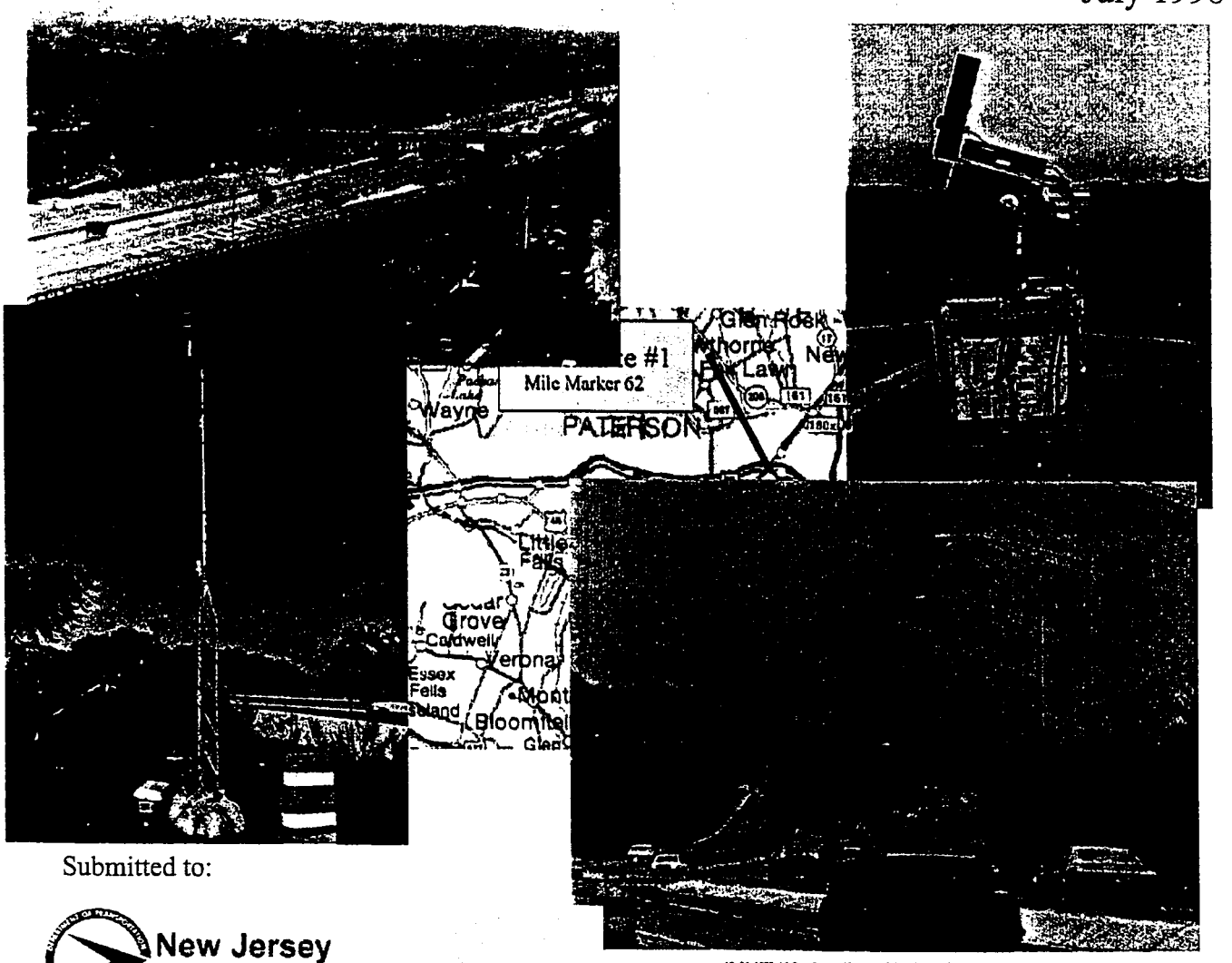

Submitted to:

New Jersey Department of Transportation

Submitted by:

Santa Fe Technologies
University of Iowa
Los Alamos National Laboratory
IBM

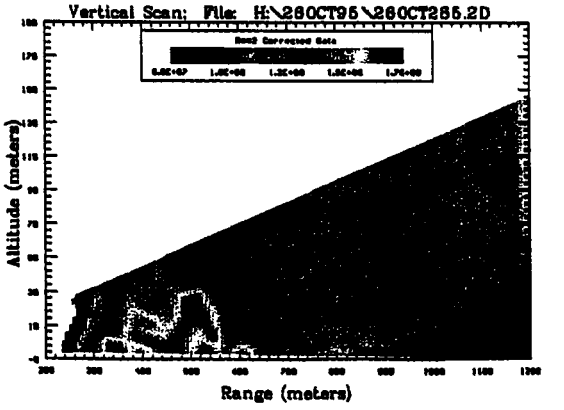

NOTICE

The United States Government does not endorse products or manufacturers. Trade or manufacturers' names appear herein solely because they are considered essential to the object of this report.

DISCLAIMER STATEMENT

The contents of this report reflect the views of the author who is responsible for the facts and accuracy of the data presented herein. The contents do not necessarily reflect the official views or policies of the New Jersey Department of Transportation, or the Federal Highway Administration. This report does not constitute a standard, specification, or regulation.

Technical Report Documentation Page

1. Report No.	2. Government Accession No.	3. Recipient's Catalog No.
FHWA/NJ-98-004		

4. Title and Subtitle	5. Report Date
The Use of Lidar to Evaluate Existing Incident Management System on I80 in Morris, Essex, and Passaic Counties in Northern New Jersey	June 1998
	6. Performing Organization Code
7. Author(s)	8. Performing Organization Report No.
William Eichinger and Howard Kraye	98-004-7290
9. Performing Organization Name and Address Santa Fe Technologies 2021 Girard S.E. Suite 201, Bldg. 2 Albuquerque, NM 87196	10. Work Unit No. (TRAIS)
	11. Contract or Grant No. SPR Research Study 7290
12. Sponsoring Agency Name and Address New Jersey Department of Transportation Bureau of Quality Management Services 1035 Parkway Avenue Trenton, NJ 08625	13. Type of Report and Period Covered Final Report Sept. 1995 - June 1998
	14. Sponsoring Agency Code

15. Supplementary Notes

16. Abstract

Measurements of carbon monoxide and particulate emissions were made of incidents (situations on or near the highway which have the effect of blocking or delaying traffic on I80) during a one week period in October, 1995. An elastic scattering lidar was used to measure the particulate concentrations over the large portions of the interstate in two dimensions.

The results from this measurement campaign indicate that the ambient concentrations measured over the highway (in the case of the lidar) or near the roadway (in the case of the CO monitors) during an incident varies from three to ten times those found in nearby locations not directly influenced by emissions from the traffic flow. The concentrations found over the roadway during normal traffic flow are approximately 35% higher than those found in the nearby air.

The resulting conclusions are 1)the implementation of an incident management system that reduces the severity and duration of the effects on traffic flow will also result in improved air quality; and 2) the amount of improvement in air quality is difficult to quantify due to the lack of quantifiable traffic data (vehicle number, type, and speed) with which to correlate the pollutant concentration data.

In order to quantify the amount of benefit to be gained from the implementation of MAGIC, a two-week measurement campaign is recommended that specifically targets high accident areas on the interstate as well as makes similtaneous traffic and pollutant measurements.

17. Key Words	18. Distribution Statement
Urban Air Pollution, Highway, Lidar, Congestion Management	No Restrictions

19. Security Classif. (of this report)	20. Security Classif. (of this page)	21. No. of Pages	22. Price
Unclassified	Unclassified		

Form DOT F 1700.7 (8-72) Reproduction of completed page authorized

TABLE OF CONTENTS

The Use of Lidar to Evaluate Existing Incident Management System on I-80 in Morris, Essex, and Passaic Counties in Northern New Jersey

SUMMARY AND CONCLUSIONS

Measurements of carbon monoxide and particulate emissions were made of incidents (situations on or near the highway which have the effect of blocking or delaying traffic on I-80). The measurements indicate that the ambient concentrations measured over the highway (in the case of the lidar) or near the roadway (in the case of the CO monitors) during an incident varies from three to ten times those found in nearby locations not directly influenced by emissions from the traffic flow. The concentrations found over the roadway during normal traffic flow are approximately 35% higher than those found in the nearby air.

The lidar data taken in this campaign are measurements of the particulate concentration along two dimensional "slices" that are horizontal or vertical planes through the atmosphere. The

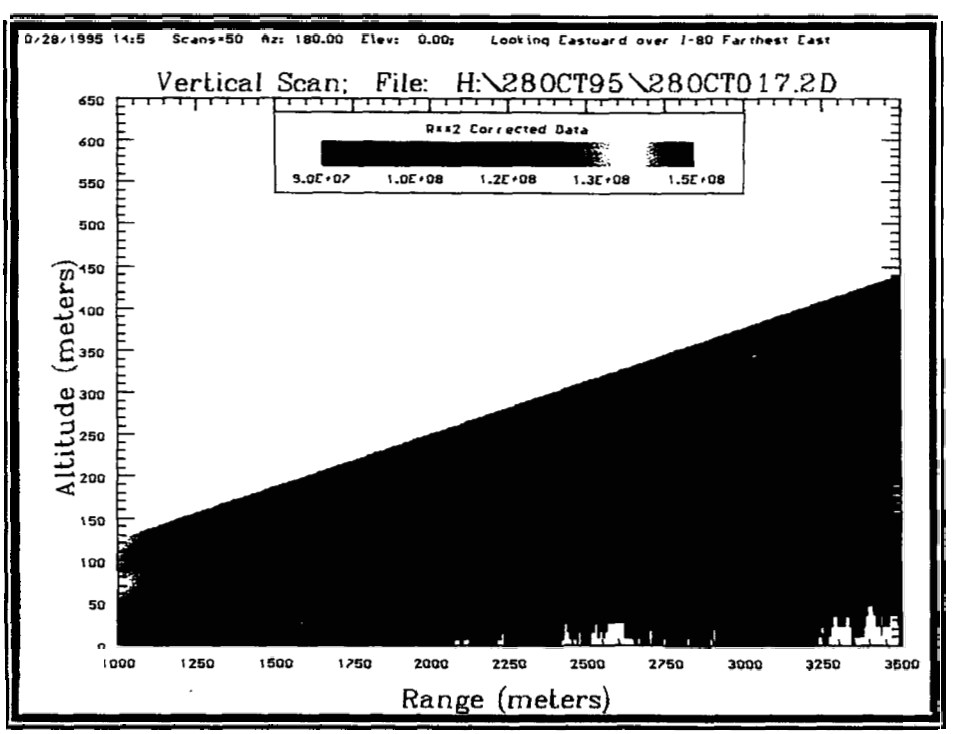

Figure 1: An example of a vertical lidar scan. Blue colors represent low particulate concentrations, red is highest. Sources of particulates can be found at 1550 meters, 2900 meters and 3150 meters.

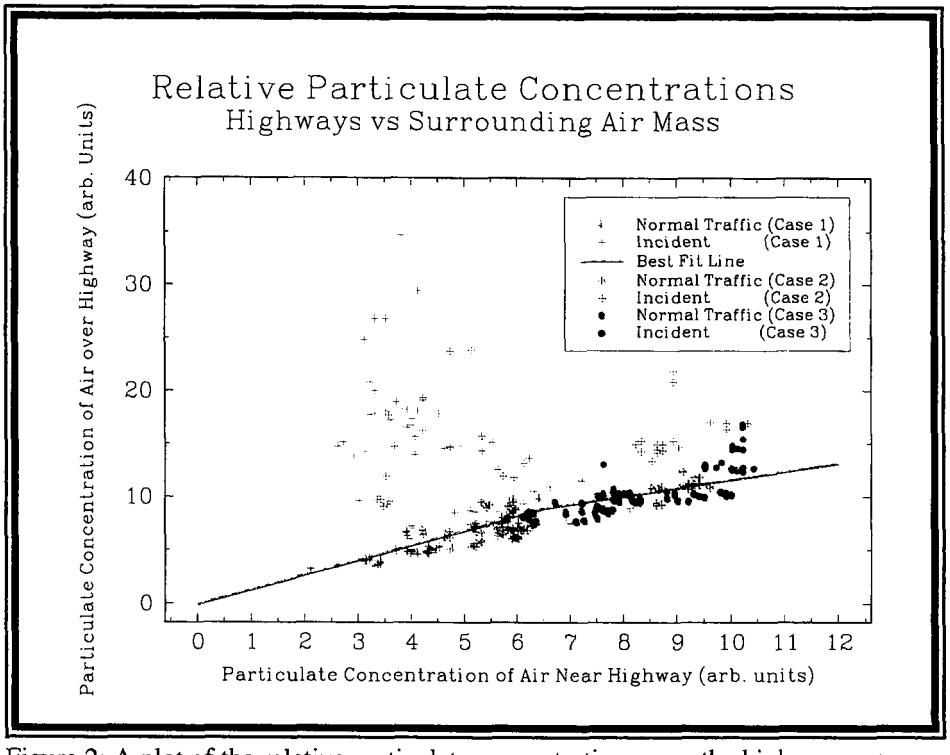

Figure 2: A plot of the relative particulate concentrations over the highway as a function of the ambient concentration. Data from traffic incidents are shown in red.

plots of lidar data are graphical depictions of the intensity of the lidar return signal in two dimensions, corrected for range and average attenuation effects (for example, see figure 1). The data shown in this report are proportional to the absolute particulate concentrations and show relative concentrations. Three case studies were performed of incidents on I-80 in which the data were examined in detail. The data demonstrate that traffic incidents can be clearly identified using lidar backscatter returns and comparing the abnormally high concentrations of particulates as compared to the concentrations found in the air nearby. Figure 2 is a graph comprised of data from the three case studies showing the difference between roadway concentrations during normal and incident levels of traffic as compared to the ambient air concentration. Under normal traffic conditions, the particulate concentration over the roadway is about 35% higher than the ambient air. As the ambient loading increases, the relative increase in concentration over the roadways decreases until the amount of relative increase is small (right side of the graph). However, during an incident, the concentration is generally 3 to 10 times higher. This allows a simple method of discriminating between normal and incident traffic on the basis of the particulate concentration over the roadway which can be measured remotely. This simple method has been shown to work in poor weather situations in which the weather was intermittently foggy with low level clouds.

It can be shown that the concentration of a pollutant near a source is proportional to the rate of emission of the particular pollutant [for example, Sutton, 1954; or Seinfeld, 1986]. The

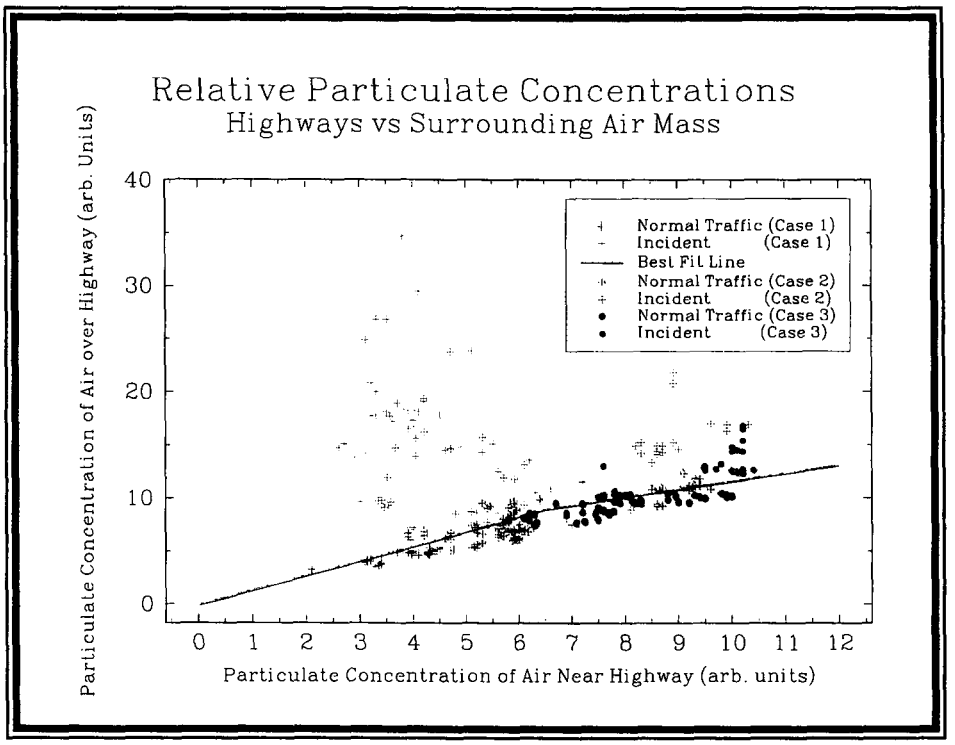

Figure 2: A plot of the relative particulate concentrations over the highway as a function of the ambient concentration. Data from traffic incidents are shown in red.

plots of lidar data are graphical depictions of the intensity of the lidar return signal in two dimensions, corrected for range and average attenuation effects (for example, see figure 1). The data shown in this report are proportional to the absolute particulate concentrations and show relative concentrations. Three case studies were performed of incidents on I-80 in which the data were examined in detail. The data demonstrate that traffic incidents can be clearly identified using lidar backscatter returns and comparing the abnormally high concentrations of particulates as compared to the concentrations found in the air nearby. Figure 2 is a graph comprised of data from the three case studies showing the difference between roadway concentrations during normal and incident levels of traffic as compared to the ambient air concentration. Under normal traffic conditions, the particulate concentration over the roadway is about 35% higher than the ambient air. As the ambient loading increases, the relative increase in concentration over the roadways decreases until the amount of relative increase is small (right side of the graph). However, during an incident, the concentration is generally 3 to 10 times higher. This allows a simple method of discriminating between normal and incident traffic on the basis of the particulate concentration over the roadway which can be measured remotely. This simple method has been shown to work in poor weather situations in which the weather was intermittently foggy with low level clouds.

It can be shown that the concentration of a pollutant near a source is proportional to the rate of emission of the particular pollutant [for example, Sutton, 1954; or Seinfeld, 1986]. The

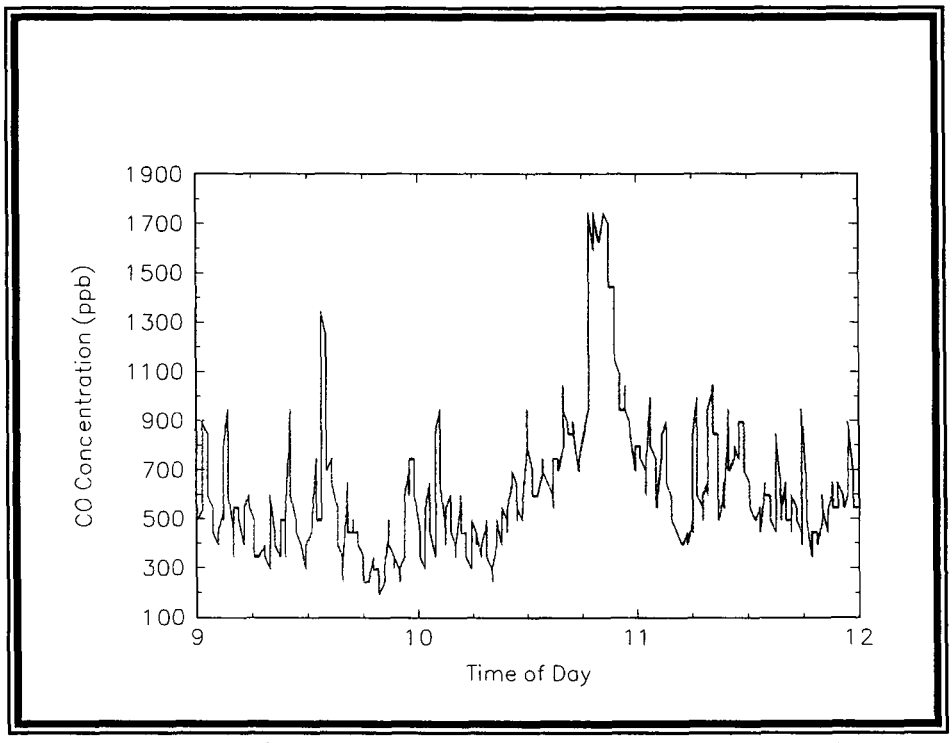

Figure 3: A plot of the CO concentration measured by CO monitor #1663 during the period of an incident. Note that the peak just before 1100 hours is three to four times the concentration before or after the incident.

data shown here imply that the emission rates of particulates is several times higher during incidents. This conclusion is also borne out by studies showing that the amount carbon monoxide emitted per mile increases dramatically with decreasing speed [Sturm et al, 1997]. NO_x emissions also tend to increase, but with far more spread in the data. Also significant is that a major factor in the emission rates for automobiles is the presence or absence of acceleration. Changes in vehicle speed generally result in increasing emission of pollutants. Thus the data shown here are consistent with previous measurements of vehicle emission rates

Measurements of carbon monoxide (CO) were also made at various points along the highway. These fast response sensors captured higher levels of CO from several of the incidents identified by HNTB. One example is shown in figure 3 from one of the sensors (serial #1663) for an incident that occurred nearby on the morning of 28 October at approximately 1100 hours (State Police #825915). (The times of the incidents are given only to the nearest hour.) The sensor was less than a mile from the official location of the incident. Again, one notes that the CO concentration rose by approximately a factor of 4 over what was present prior to the incident. Thus the CO measurements confirm the results obtained from the lidar that the pollutant levels during incidents are several times greater than normal levels.

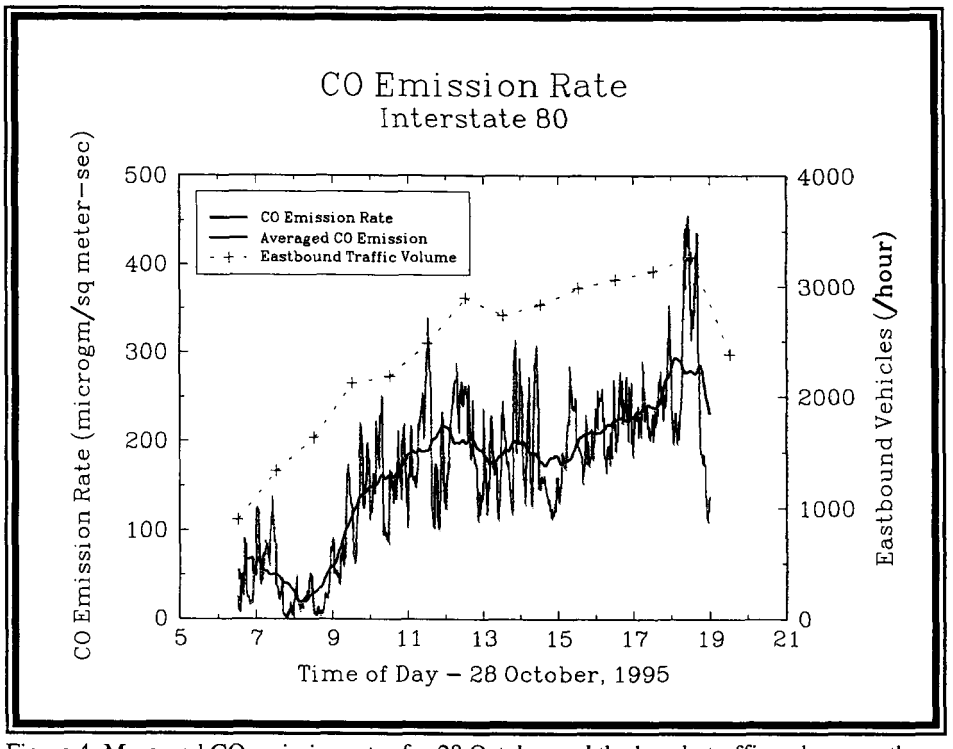

Figure 4: Measured CO emission rates for 28 October and the hourly traffic volume on the eastbound lanes of I-80. The dark solid line is the smoothed emission rate.

Because the concentration of a given pollutant at any location is a function of both the emission rate and the weather, it is impossible to determine absolutely the effectiveness of a given remediation program using only concentration data. Thus, methods must be developed to determine the emission rates.

The CO emission rates shown in figure 4 were measured on 28 October, 1995 using an innovative new technique first demonstrated during this project. Details of the technique may be found in Appendix E. The measured rates can be compared to estimates based upon the emission rates of CO from an average vehicle and the traffic volume during the day of the measurements. The measured emission rate lies between the emission rate of CO from an average vehicle as given by the National Vehicle and Fuel Emissions Laboratory of the EPA (EPA, 1997) as approximately 22 grams of carbon monoxide per mile and the emission rates described by Cicero-Fernandez and Long [1997] and Sturm et al. [1997] which range from 4 g/mile to about 8 g/mile. A value of 6 g/mile results in an emission rate of about 125 micrograms/m^2-s. The data presented here lie between these two extremes.

RECOMMENDATIONS

It is clear that the implementation of an incident management system that reduces the severity and duration of the effects on traffic flow will also result in improved air quality. Thus

the implementation of this system should be encouraged for air quality reasons as well as for the benefits to commuters.

The amount of improvement in air quality is difficult to quantify with the data collected during this project. This is primarily due to the lack of numerical traffic data (number of vehicles, type, and speed) with which to correlate the pollutant concentration data. While the type of data collected by HNTB provides anecdotal information on some incidents, it is not complete, nor coincident with lidar data collection, nor are there quantitative data which can be used for correlation with measured pollutant concentration levels.

In order to quantify the amount of benefit to be gained from the implementation of MAGIC, measurements are required of the number and average velocity of the vehicles on the highway. These measurements are required at several points on the highway and coordinated with measurements of the primary pollutants. An improved method of communicating the existence of incidents between the measurement teams would also be beneficial. Some method of notification from the state police of the existence of an incident in real time would be especially desirable.

Concentration of the measurement campaign on those parts of the highway in which accidents are most prevalent would be most productive. While aircraft photography of the highway may offer several qualitative advantages and viewing of extended parts of the interstate, because of the proximity of Teterboro Airport, the easternmost sections of the highway cannot be examined. This part of the highway has the worst air quality and the highest incident rates and thus offers the best opportunity to observe the largest number of incidents.

The use of the pollutant emission rate technique developed during this campaign with traffic measurements on both sides of the highway would also be of use in determining the benefits to be accrued from implementing MAGIC. Because the technique can be used to correlate the number of vehicles and their speed with the emission rate of CO, one can directly assess the effect on local air quality of the MAGIC system. At this writing, SFT can deploy three of the measurement systems.

Because the amount and duration of incidents are highly variable, an extended measurement campaign would provide more data and more reliable results. A measurement period of two weeks is recommended.

INTRODUCTION

Objectives

The Incident Management System (IMS) project is aimed at improving mobility and transportation productivity, enhancing safety, making optimum use of existing transportation facilities and energy resources, while also addressing environmental requirements. Improving the environment is a key objective of Transportation Improvement Plans (TIP) and is a focus for State Implementation Plans (SIP). NJDOT is committed to applying the benefits of advanced technology to highway transportation and recognizes the potential for reducing harmful emissions by improving current transportation systems and by creating more progressive systems. In order to quantify the air-quality benefits of the implementation of IMS, a baseline survey over areas in the MAGIC corridor will be focused over areas that have a high probability of incidents. The following objectives were addressed:

* evaluate the effectiveness of the I-80 MAGIC Incident Management System by collecting air pollution data prior to the installation.
* evaluate the potential benefit of lidar in terms of quality, accuracy, ease of use, and data interpretation as a tool for management of the IMS.
* measure the relationship between congestion on I-80 and the ambient air quality in the study area.

Background or History

Improving the environment is an important objective in the design and development of Intelligent Transportation Systems (ITS). The Clean Air Act Amendment of 1991 (CAA) and the Intermodal Surface Transportation Efficiency Act (ISTEA) have placed more demands on metropolitan areas to develop surface transportation plans that will contribute to the improvement of air quality. The State of New Jersey is installing an IMS in order to mitigate the effects of traffic accidents and incidents have on traffic flow. Evaluation of the effect this system will have on air pollution was accomplished using remote sensing lidar (LIght Detection And Ranging) technology in coordination with conventional point instruments.

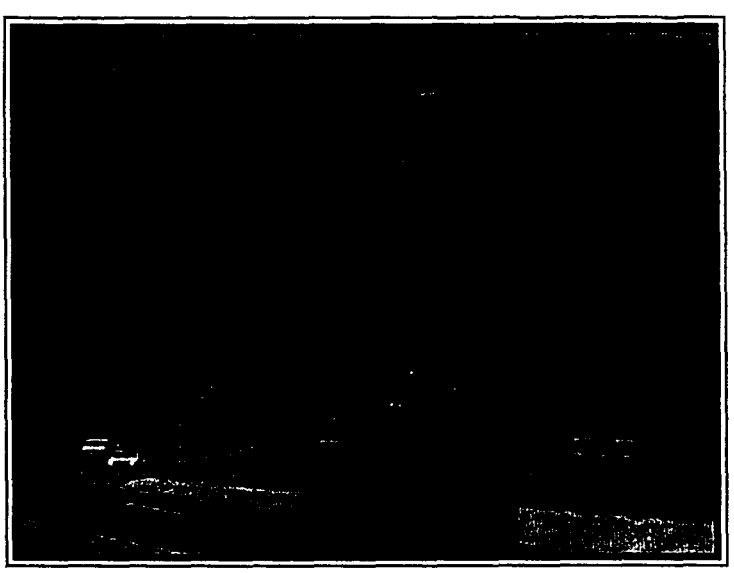

Figure 5: The view of Interstate 80 from lidar site #2 looking towards New York.

The Light Detection and Ranging (lidar) systems used in New Jersey are laser based scanning systems that are capable of monitoring the sources and the transport and dilution of the particulates in real-time. The system can detect and track plume sources over a large area and present 2-D and 3-D images superimposed on a GIS area traffic map.

The lidar system was fielded in conjunction with mobile traffic evaluations and fixed traffic counters operated by Howard Needles, Tammen and Bergendoff (HNTB), and point instruments (measuring CO, temperature, relative humidity, wind speed and direction) fielded by Los Alamos National Laboratory (LANL), Santa Fe Technologies (SFT), and the New Jersey Department of Environmental Protection (NJDEP) at one or more sites along Interstate 80 (I-80) in the Metropolitan Area Guidance Information Center Corridor (MAGIC). The project objective was to determine the effects of IMS traffic management on air quality. This project represents a partnership between the New Jersey Department of Transportation (NJDOT), Howard Needles, Tammen and Bergendoff, and a team lead by SFT that includes the University of Iowa (UI), LANL and IBM. The New Jersey Department of Environmental Protection provided informal guidance and technical advice. The preliminary study (the condition prior to the installation of IMS) was done in late October, 1995.

A contract was issued between the New Jersey Department of Transportation (NJDOT) and SFT on 9 September, 1995. The SFT team performed lidar measurements in the area of I-80 during a seven (7) day period from October 23-30, 1995. Evaluations were made throughout the project to assess aspects of equipment accuracy & reliability, data acquisition, collection, storage, transfer, display and analysis.

This initiative was a unique application of lidar technology developed specifically for the transportation industry. The project uses a systems approach to the integration of lidar air-quality data by incorporating traffic data, GIS information, meteorological data, emission sensors and a unique data visualization and analysis system. By using the lidar system, a wide survey of I-80 and surrounding areas was conducted. Three dimensional imaging of the lidar

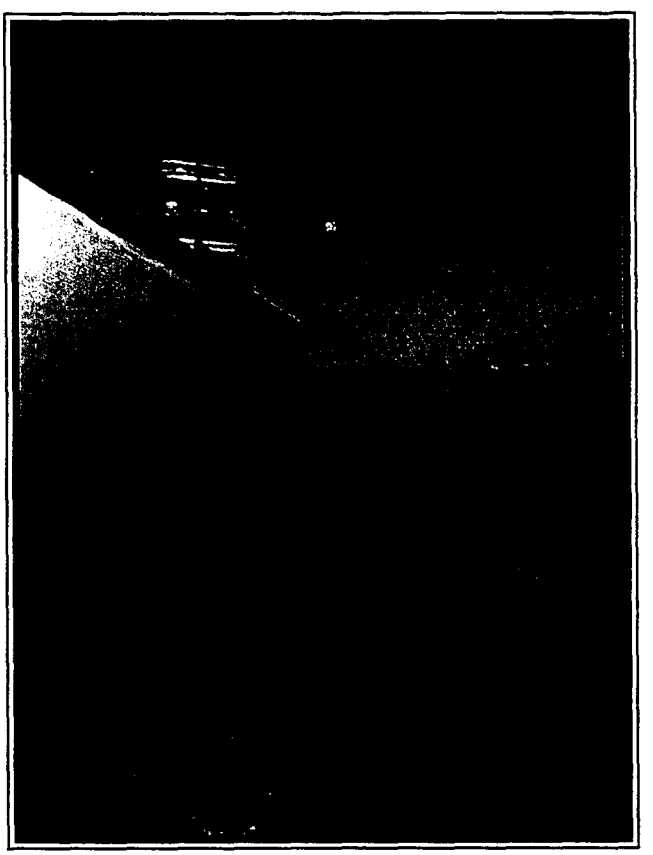

Figure 6: Setting up the lidar as dawn breaks over New Jersey. The lidar is on the roof of the Prime building at Site #3.

information was used to identify problematic areas that were then overlaid onto the GIS map. Localized air and traffic monitoring at selected locations measured specific pollutants and was used to characterize vehicle volumes. This monitoring program was intended to determine whether the IMS measures have a real impact on reducing the air quality problem.

State of the Art

1. Elastic Lidar

The miniature elastic system to be used for this project has been field proven in air-quality projects performed in Barcelona, Spain; Albuquerque, Las Cruces, and Sunland Park, New Mexico; El Paso, Texas; and Minneapolis, Minnesota. This lidar system is an infrared (IR) system primarily measuring scattered light from particulate matter in the atmosphere (Mie scattering). This system has a range of up to 10 km, with a range resolution of 7.5 meters, and is extremely effective in locating and tracking particulate "clouds". The particulates can be water droplets, dust, smog, smoke, carbonous particulates (exhaust) from vehicles or factories, or any other source of particulate matter. This system does not identify the chemical composition of the scattering centers, but associates particulate concentrations with the spatial location of pollution sources. Originally developed by LANL for defense applications, the technology has been made available for commercial uses. The lidar system has been recognized by Popular Science as a "Best of What's New" in environmental science and is a winner of the 1993 R&D 100 award as one of the 100 best developments that year. The use and operation of the lidars are explained in more detail in Appendix D of this document.

2. Traffic Monitoring

An assessment of the traffic conditions was made by HNTB. Six vehicles were fielded to provide real-time, on location information about traffic flow, road conditions, and weather. One aircraft (SKYCOMP) took still photos and videos of the traffic in the test area. HNTB provided information on the categorization of incidents by type. Unfortunately, few incidents identified by the drivers or aircraft were reported in real time so that intensive scanning and data collection could occur, and the traffic data from the drivers notes provided were not self-consistent and thus were not used in this analysis. All of the incidents that occurred during the study period (as

Figure 7: A picture showing the location of one of the carbon monoxide sensors along Interstate 80. The sensor can be seen on the post just under the Emergency Phone sign..

reported by the state police) are listed in appendix E. It should be noted that the list of incidents from the state police may not be complete. For example, the traffic slowdown observed in case study III (appendix C) is not listed by the police but was observed to occur. This may be because the official interest is more toward accidents than occurances that the police cannot control or affect even though they may cause disturbance to the traffic flow.

3. CO/ Meteorological Monitors

SFT deployed eight portable carbon monoxide (CO) monitors at a number of sites along I-80. The CO monitors are Langan Products L-15 portable sensors. The L-15 sensors measure minute by minute temperatures and CO levels down to 50 parts per billion (ppb). The sensors were routinely tested and re-calibrated (if necessary) using test gases with concentrations of 0.0, 10.0, and 60.0 ppm CO. During the course of the project, each instrument was calibrated on four separate occasions. While these CO sensors are not EPA certified, they are able to make measurements of the CO concentration on time scales as short as 30 seconds. Thus they are useful for monitoring the effects of short term fluctuations in the traffic flow. It was hoped that the placement of the sensors would enable detection of the effects of incidents on local CO concentrations.

Two CO monitors were mounted at two different heights on a 6 meter tower with a three dimensional sonic anemometer, and two temperature-humidity probes. The sonic anemometer was used to determine the ambient wind speed, direction, the sensible heat flux (a measure of the amount of heat added to the atmosphere) and the vertical momentum flux (a measure of the vertical mixing in the atmosphere). The two temperature humidity probes were used in a Monin-Obukov similarity analysis to estimate the latent and sensible heat fluxes which in turn enable the determination of CO fluxes as a similarity scalar. Appendix E contains details of the methodology used to determine the CO flux.

4. RISC 6000 Rendering System

SFT/IBM provided an IBM Reduced Instruction Set Computer (RISC) series 6000 as the rendering system. The computer workstation has the necessary processing and memory capability to run the Data Explorer™ software environment which is used to integrate various types of information into a centralized control and display interface system.

The NJDOT digitized Geographic Information System (GIS) location information was incorporated into the database and lidar images were scaled and superimposed onto maps of the various sites. Additional data from the air-quality sensors, traffic condition sensors, and meteorological conditions were also displayed as overlays or pop-up windows. Data which comes from particular locations, such as the traffic, or CO concentration data, is displayed at the position where it was taken. The data were processed off-line into the rendering system by IBM and SFT and shown to NJDOT personnel several months after data collection.

Project Locations

A complete listing of project sites and the locations of each of the monitors is given in Appendix B. The map above shows the pertinent portions of Interstate 80 and the locations of the three lidar sites.

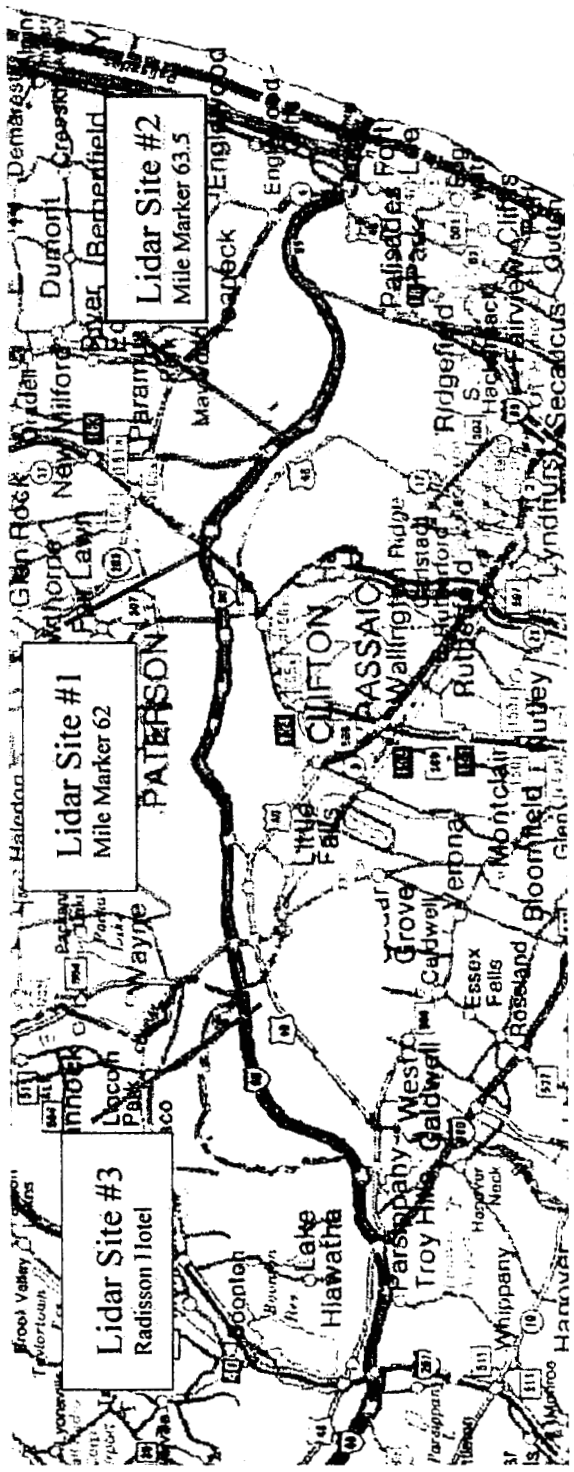

8Figure 8: A map of the eastern portion of I-80 in Northern New Jersey. The three lidar sites are marked.

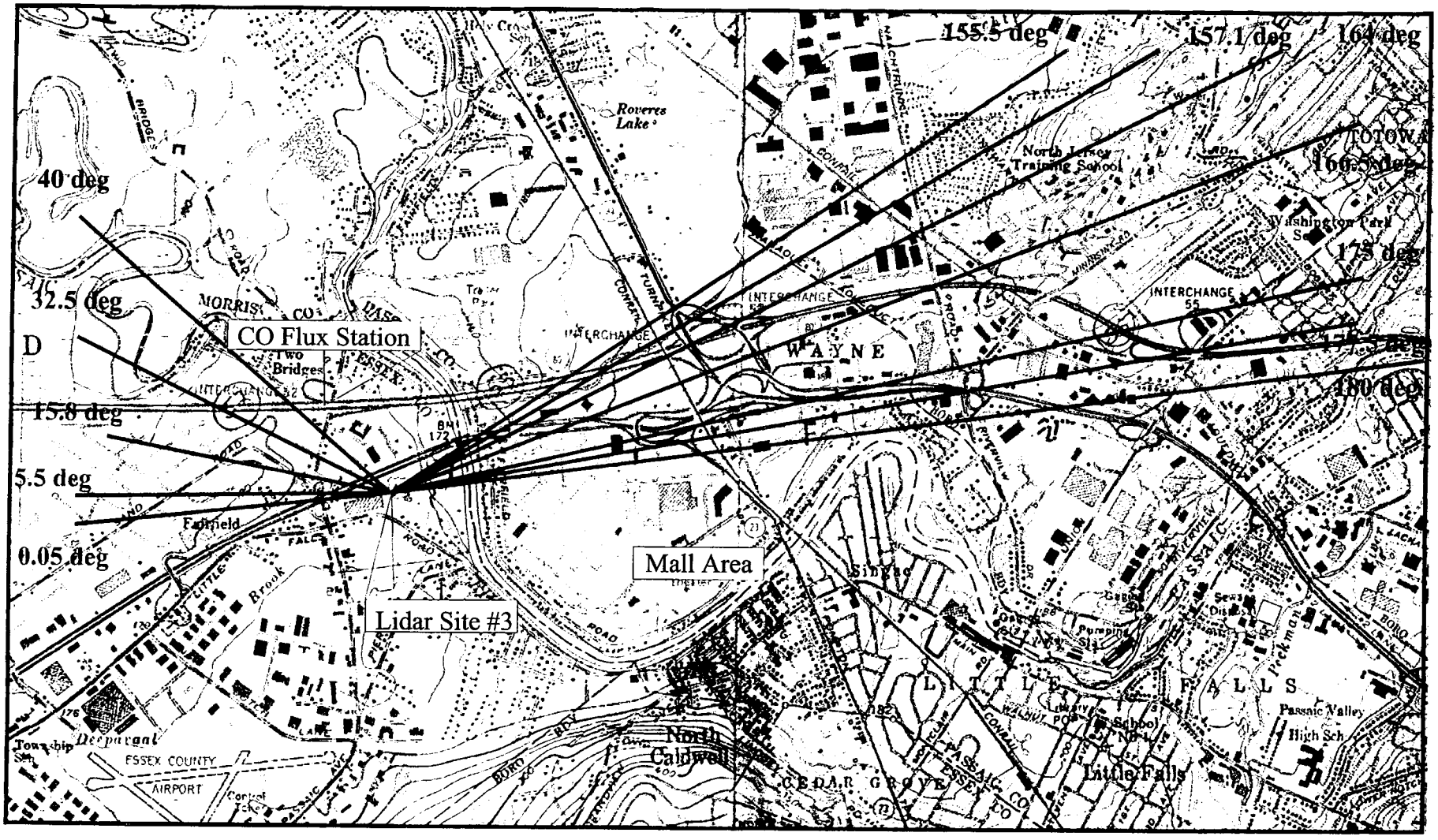

Figure 9: A map of part of I80 near Lidar Site #3 with the azimuths of the normally executed lidar scans designated. The angles given are in the lidar coordinate system. North is up.

STUDY PROCEDURES

Data Collection

Data collection during the campaign was generally conducted from 0830 hours until 1800 hours daily. Exceptions were caused by instrument malfunctions, changing sites, and inclement weather (rain washes the pollutants from the air extremely rapidly so remote sensing of them is not possible).

A combination of vertical, horizontal and three-dimensional lidar scans were periodically executed. The direction and type of scans were determined by the location of the areas of interest on the highway. Vertical scans (which display the concentration in a vertical slice of the atmosphere) show the existence and concentration of the plumes over the highway. Horizontal scans (which display the concentration in a horizontal slice of the atmosphere) show the extent of the incident, often showing traffic backed up at on/off ramps and on supporting highways. The sequence of scans was programmed into a file that was repeatedly executed by the lidar.

The time between cycles was determined by the number of scans and the volume of space covered by the scan sequence. The small size of the lidar beam allows high spatial resolution, but it also means that only a small volume of space can be explored with every laser pulse. The number and type of scans that were executed were selected so as to best cover the area of interest. The scan sequence was executed and restarted immediately upon completion of the last scan. In this way, the maximum amount of area is covered with as many "snapshots" of the conditions as possible and thus the likelihood of observing an incident was maximized. A typical sequence took approximately 20 minutes to complete.

As an example of the way in which lidar scans were selected to cover likely incident areas, figure 9 is a map of the area near Lidar Site #3 emphasizing the roads to the east of the site. For clarity, only the vertical scan sequences are shown. Note that all of the on/off ramps on I-80 and Route 46 have scans above or near them. In some cases the angles are not ideal because they must be offset somewhat because of an obstruction (trees, power lines, or buildings). Many of the flat, open stretches of the highways have scans above them as well. Horizontal scans are also done to capture the same areas to show the spatial extent of the problem areas. The area coverage of the horizontal scans were limited in spatial extent to about 15 degrees at Lidar Site #3 because of a large number of trees near the site that required that the scans be broken up into smaller pieces.

Carbon Monoxide monitors were placed along the highway at sites near which incidents were anticipated to occur (near on/off ramps, road obstructions, changes in the roadway, etc) Data collection from the CO monitors was nearly continuous during the campaign. Exceptions include calibrations, changing sites, and equipment malfunctions (caused primarily by rain on the electrical connections). Data were taken at one minute intervals and stored on the monitor. Data were downloaded to a computer daily.

Deployment

Thursday, 19 October: Arrival of personnel from SFT and LANL
Friday, 20 October: Final coordination / pick up, and check lidar systems
Saturday, 21 October: Preliminary examination of Sites
Sunday, 22 October: Set up on I-80 at Site #1
Monday, 23 October: Start the highway project
Tuesday, 24 October: Set up on I-80 at Site #2
Thursday, 26 October: Set up on I-80 at Site #3
Monday, 30 October: Finish highway project

Data Reduction

The plots of lidar data that are displayed are graphical depictions of the intensity of the lidar return signal in two dimensions. The signals have been corrected for range and average attenuation effects. It has been shown that the backscatter signal from a 1.064 micron lidar tracks the concentration of particulates with diameters in the range of 0.5 to 2.5 microns [Hofeldt and Olson, 1997; Chakravarty et al., 1995a, 1995b]. Thus while the data shown in the three case studies is not a direct measure of the concentration of particulates, the variations in the lidar return do represent variations in the overall particulate concentrations. Recognizing that there are several limitations to this approach (that will be pointed out as they occur), the lidar data will be treated as proportional to the particulate concentrations and the plots as maps of the relative particulate concentrations.

The intensities of the lidar returns are depicted as colors in the plots. Higher intensities that correspond to higher particulate concentrations are shown as red. Similarly, lower intensities that correspond to lower particulate concentrations are shown in blue. The color bar on each plot shows the color changes from red to blue and shows the values of the lidar intensity so that quantitative comparisons can be made. All of the plots shown in Cases I through III were taken using the same instrument settings, so that the lidar intensities can be compared from plot to plot.

Most of the scans that are shown are vertical scans (also known as RHI (range-height indicator) scans). They are taken by pointing the lidar in a given azimuth and taking data successive elevation angles. The result is a plot of the of the particulate concentration in vertical slice the atmosphere. One may also perform a horizontal scan in which the elevation angle is held constant and the azimuthal angle is changed. Unless otherwise stated, one may assume that the plots shown represent a vertical scans of the relative particulate concentrations in the atmosphere.

It interpreting the plots, it is important to note that nearly all of the plots are exaggerated in the direction perpendicular to the lidar's line of sight (in the vertical direction for a vertical scan and in the horizontal direction for a horizontal scan). This is because the range of the lidar is generally very long with respect to the size of the objects that we are attempting to find. Expanding the dimension perpendicular to the lidar's line of sight often allows one to examine a scan in more detail. For example, figure 10 is a vertical scan from Lidar Site #3 looking to the east in which the horizontal and vertical scales are equal. The structures that one observes are rounded and shapes similar to what one observes smoke plumes to look like.

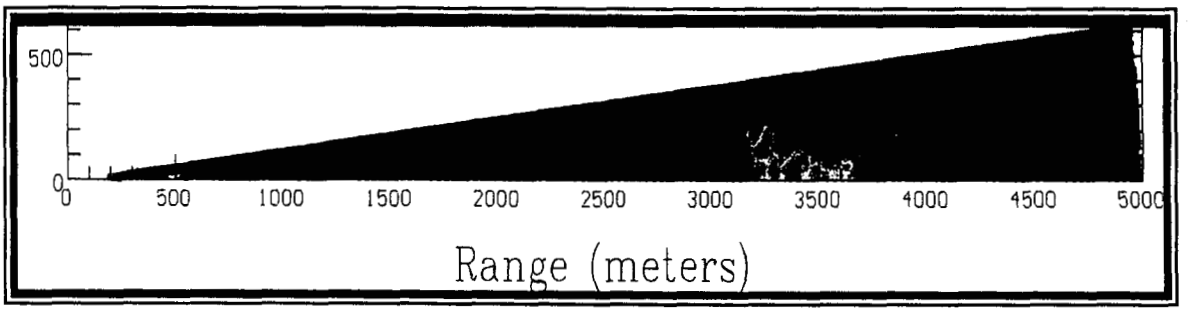

Figure 10: A map of the particulate concentration using an aspect ratio of 1:1, that is, a distance along the horizontal dimension represents the same physical distance as in the vertical dimension.

In contrast, figure 11 is a plot of the same data but with the vertical dimension expanded. One can now see a number of plumes near the ground that were not clearly visible in figure 10 (for example, at 2000m, 1100m, 800m, and 600m). However, expanding the plots will occasionally distort the plumes to the point where they appear unnatural, or it may expand structures to the point where the data appears to be "noise". For example, the data to the right of the plume at 3500 meters could be interpreted as "noisy", but examination of the plot at normal aspect ratios shows the variations as normal disconnected structures that are often found in the atmosphere. Another, more extreme, example can be found in figure 12 below. Because the range resolution in the dimension perpendicular to the lidar line of sight increases with range, this results in decreasing visual resolution at longer ranges. Thus the problem of distortion becomes worse at longer ranges.

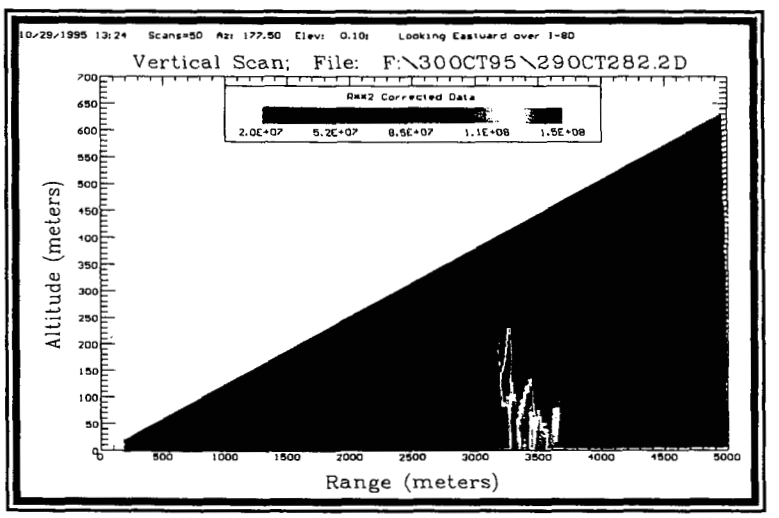

Figure 11: A map of the particulate concentration using an aspect ratio of 4:1. A distance along the horizontal dimension represents 4 times the same physical distance a similar distance in the vertical dimension. In other words, the vertical dimension has been expanded to reveal details not otherwise clear.

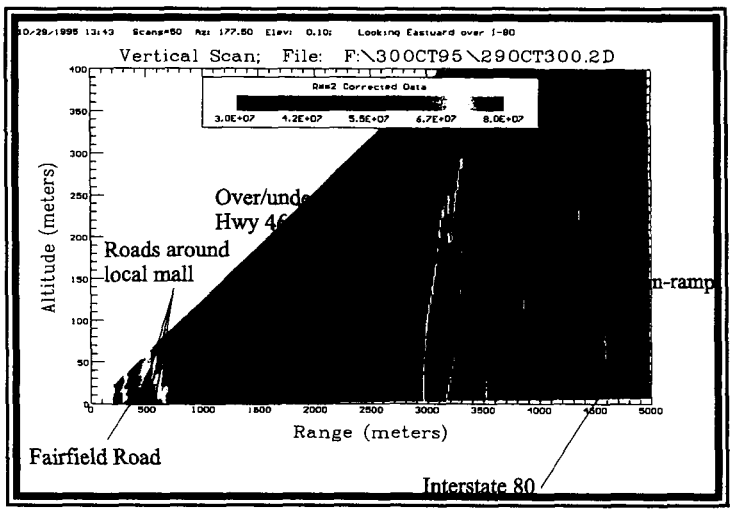

Figure 12: A lidar plot of the area to the east of Lidar Site #3. The plot is annotated with the locations of several major sources of particulates.

Because the lidar images depict the changes in particulate concentration, it is not surprising that one can locate ground locations, like roads and parking lots, in which particulates are generated. Figure 12 is an example of a plot in which the locations of major roads are shown on the plot. The correspondence between the location of the plumes from the surface and the location of the roads/highways is quite good. Compare the locations of the indicated plumes with the map shown in figure 9 and the line of sight indicated for 177.5 degrees.

Analytical Method

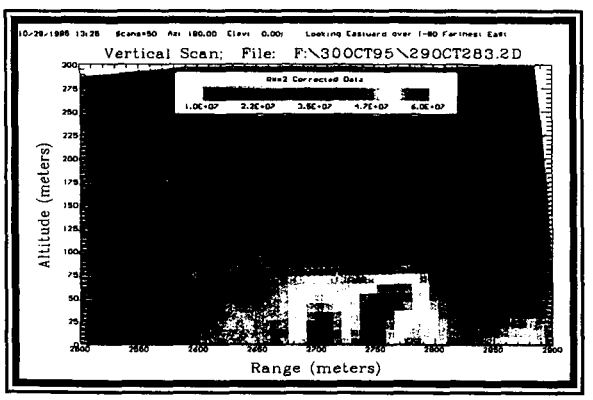

Figure 13: A blow-up of the area around 2700 meters to the east of Lidar Site #3 as shown in figure 12. Two distinct plumes can be seen coming from the surface.

Because of the high spatial resolution of the lidar, the locations of particulate sources can be located quite precisely. Figure 13 is a blow up of the region around 2700 meters to the east of Lidar Site #3. This corresponds to a somewhat complex area where several roads intersect, notably the Naactpunkt/Riverview Roads and Minnisink road intersections with Route 46 (see map in figure 9). While in the New Jersey Project the data was taken with 7.5 m range resolution, the instrument is capable of 1.5 meter resolution. Thus improvements by a factor of five over the resolutions shown here are possible.

An incident as used in this report is defined as an occurrence that results in traffic being stopped or slowed. This may be the result of an accident or just some activity along the highway that causes drivers to stop or slow down to observe. HNTB did not report this incident.

The incident that is being examined here is an accident that occurred in the vicinity of the on ramp from Route 46 onto I-80 to the east of Lidar Site #3 on the 30th of October. The exact cause of the incident is not known, however, ambulances were observed by the lidar team on I-80 and cars were observed backed up on Route 46 and to a limited extent on I-80. The existence of

the incident was reported to HNTB by telephone when it was observed. The time the incident occurred is also not known, but an intense plume from the intersection area was first observed shortly after 1300 hrs. This plume can be seen in figure 14 and figure 15 which show slightly different locations near the intersection.

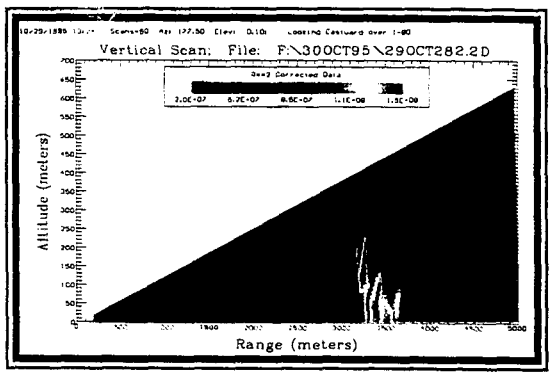

Figure 14: An incident in the area to the east of Lidar Site #3. Time is 1324 hours.

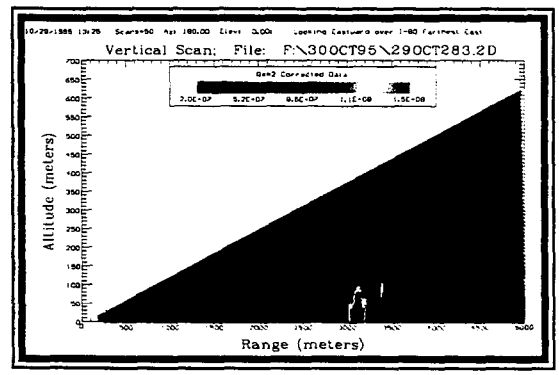

Figure 15: An incident in the area to the east of Lidar Site #3. Time is 1325 hours.

The incident responsible for the heightened emissions continued to block or slow traffic for about an hour and a half (figures 16 and 17). During this time, the intensity of the plume varied from scan to scan as did the spatial extent of the source. This is due to a combination of a variation in both the number of vehicles backed up and the intensity of the wind. After about a half hour, the incident had a significant effect on the traffic in and around the mall area (whose high speed exit is to I-80). This can be seen in the smaller plumes from 500m to 2500m in figure 17. These plumes have their origin in the access roads around the mall as well as the mall parking lot.

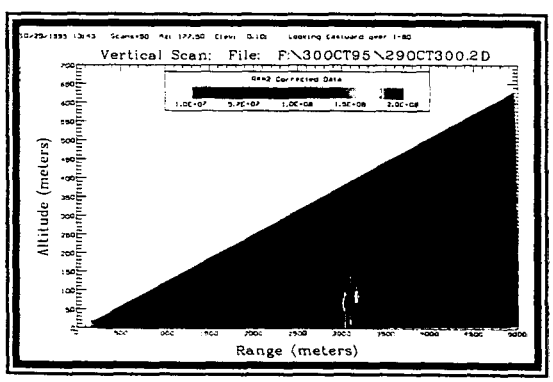

Figure 16: An incident in the area to the east of Lidar Site #3. Time is 1343 hours.

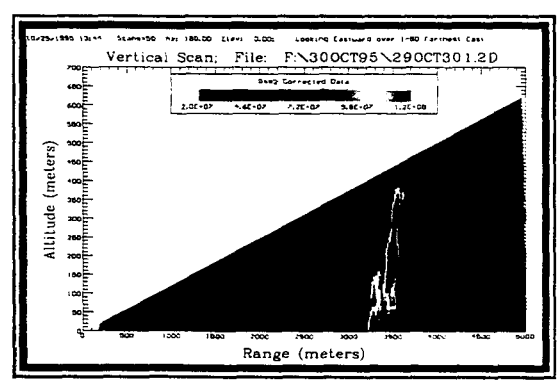

Figure 17: An incident in the area to the east of Lidar Site #3. Time is 1344 hours.

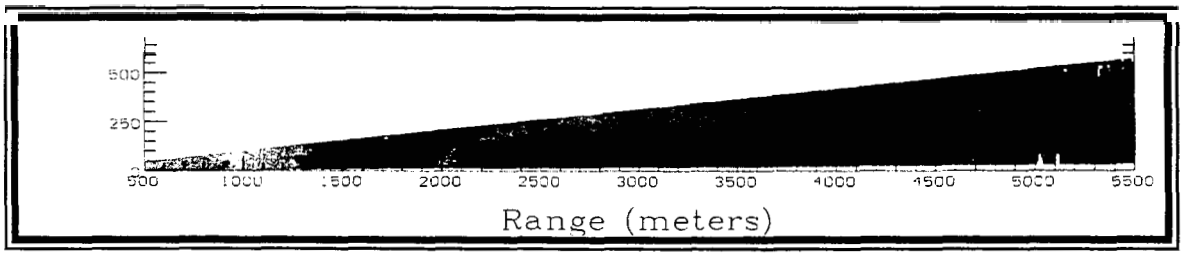

Figure 18: A horizontal scan of the air above Route 46 during the incident. One can clearly see the location of the highway by the line of increased particulates. The angular area covered by this scan is small because of trees blocking the view on either side. The time is approximately 1400 hours.

The plumes that have been shown in the previous scans have all been vertical slices of the atmosphere showing cross sections approximately perpendicular to the highway. These plumes have a large spatial extent along the highway as well as above it. Figure 18 is an example of a horizontal scan (a horizontal slice through the atmosphere) that shows the air above Route 46. A long line of increased particulates is clearly seen. At 2000 meters, the on/off ramp where Route 23 joins Route 46 can be seen as the line veers to the bottom of the graph. The intense area to the left is the mall parking lot.

By the time the incident cleared at about 1430 hours, the effect on the roads around the mall had disappeared as had the intense plume from the on ramp (figure 19). The white areas shown in the figure are areas with concentrations of particulates lower than the color bar in the legend.

Lidar data from the other two cases can be found in appendix C.

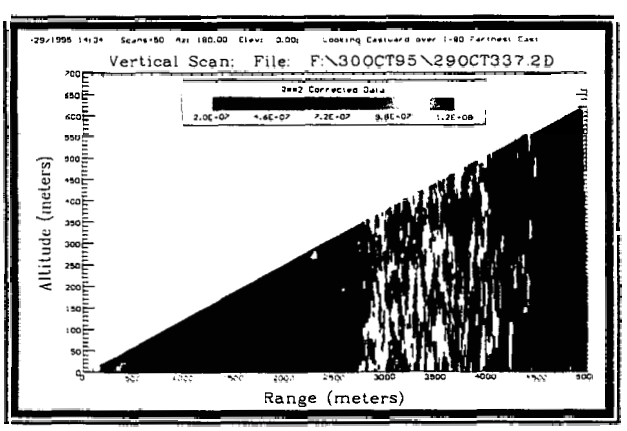

Figure 19: An incident in the area to the east of Lidar Site #3. Time is 1434 hours.

RESULTS AND DISCUSSION

Three case studies which were identified as incidents on the basis of observed traffic slow downs, show that traffic incidents can be clearly identified using lidar backscatter returns and comparing the abnormally high concentrations of particulates as compared to the concentrations found in the air nearby.

If one plots the particulate concentration (measured as the corrected lidar signal) over the highway versus the concentration of the nearby air mass but not over a particulate source, one obtains figure 20. The data in this graph was obtained from the preceding plots of lidar data.

What is interesting about the data is that for normal traffic, the concentration over the highways is about one-third greater than that over the surrounding areas while the concentration during an incident is three to ten times the concentration of the ambient air and is above a threshold value of about 10. This information allows one to set a criterion that may serve as a

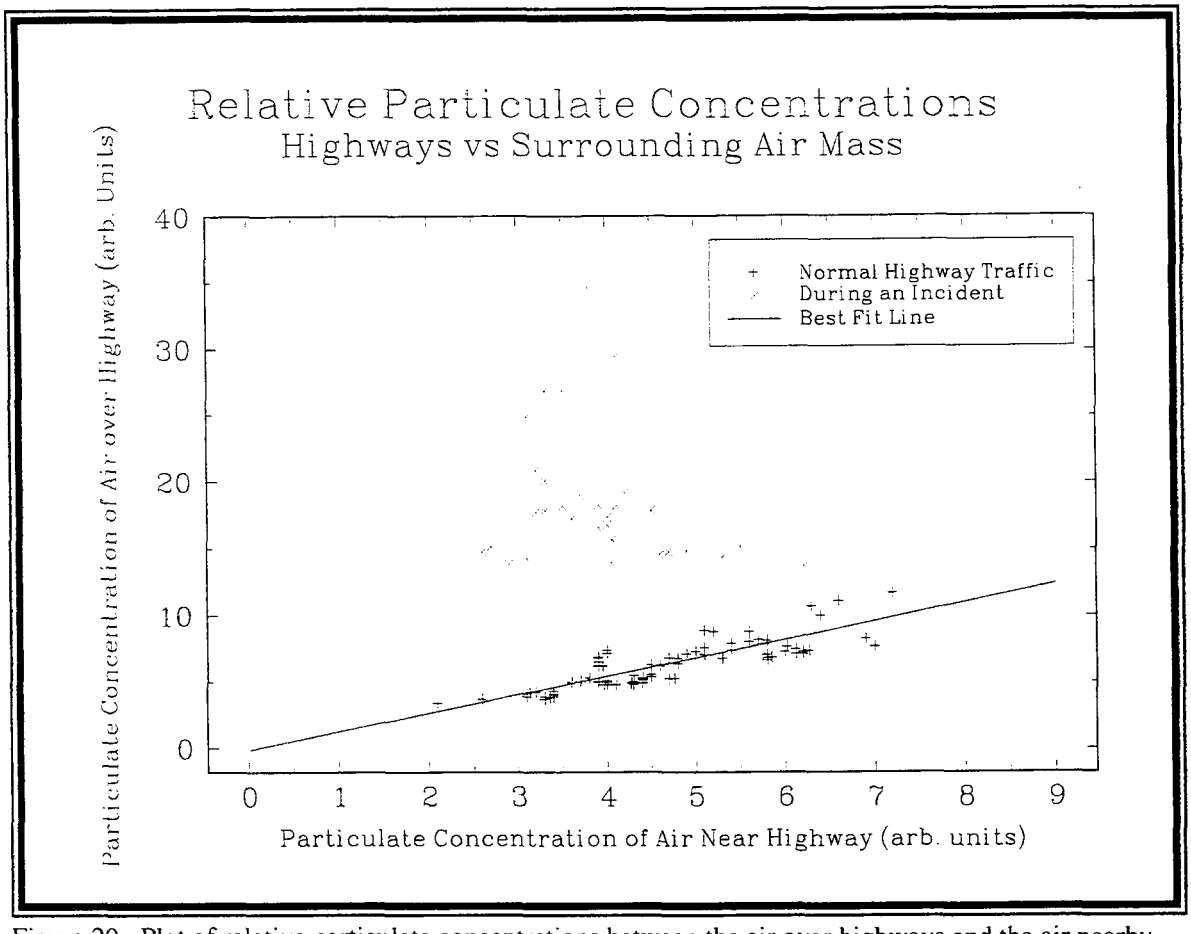

Figure 20: Plot of relative particulate concentrations between the air over highways and the air nearby not over a highway for normal conditions and during incidents.

clear indicator for incidents; one that could easily be programmed into an automated sensor network. Another conclusion that can be drawn is that incidents are a major contributor to local air pollution. Since the concentration above a source is proportional to the source strength, it follows that the source is three to ten times as great during an incident as compared to normal traffic. It has been shown that this reasoning holds for all of the primary pollutants, CO, NO, and NO_2 [Seinfeld, 1986].

Figure 21 is a composite made from all three of the case studies showing the difference between roadway concentrations during normal and incident levels of traffic as compared to the ambient air concentration. One can see that under normal traffic, the particulate concentration over the roadway is about 35% higher than the ambient air for all of the conditions except ground fog where the increase is somewhat smaller. However, during an incident, the concentration is still generally 3 to 10 times higher. This supports the concept that a simple method of discriminating between normal and incident traffic on the basis of the particulate concentration over the roadway exists and which can be measured remotely. This simple method has been

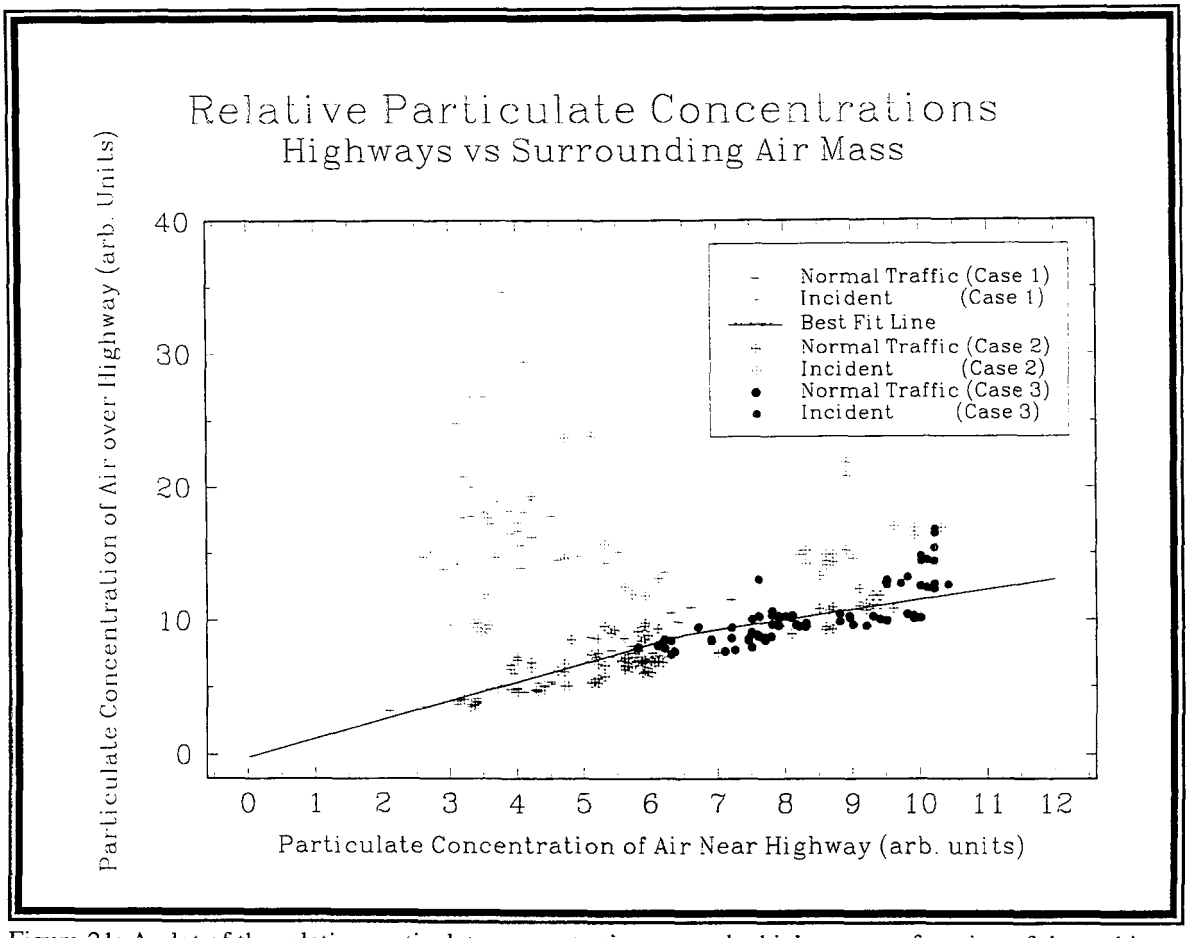

Figure 21: A plot of the relative particulate concentrations over the highway as a function of the ambient concentration. Data from traffic incidents are shown in red.

shown to work in poor weather situations in which the weather was intermittently foggy with low level clouds. In this case, the ambient air approaches those levels of concentration (caused mostly by the foggy conditions) normally found during incidents. At some point, discrimination between incidents, normal traffic, and fog conditions becomes difficult. More intelligent analysis algorithms could help (structures in fog are not generally connected to the ground while those from highways are), but there will always be a point where the fog can be sufficiently dense to obscure the surface conditions.

The results shown here are consistent with theoretical derivations that predict that the concentration of a pollutant near a source is proportional to the rate of emission of the particular pollutant [for example, Sutton, 1954; or Seinfeld, 1986]. The data shown here imply that the emission rates of particulates is several times higher during incidents. This conclusion is also borne out by studies showing that the amount carbon monoxide emitted per mile decreases dramatically with increasing speed [Sturm et al, 1997]. NO_x emissions also tend to decrease, but with far more spread in the data. Also significant is that a major factor in the emission rates for automobiles is the presence or absence of acceleration. Changing speed generally results in increasing amounts of pollutants.

If the emission rates of the various pollutants are roughly proportional, and since incidents have 3 to 10 times the emission rates of normal traffic, it stands to reason that reducing the length and impact of incidents, will help reduce local pollution concentrations. Further, any measures that are taken to keep traffic flowing smoothly will help reduce the pollutant concentrations. The amount of decrease in pollution will be dependent upon the fraction of time a particular stretch of highway experiences an incident. In some areas that are lightly trafficked, the benefit may not be great. However, those areas with high incident rates are most often those that are highly traveled. Thus reductions in pollution will occur in those areas where they are needed most.

BIBLIOGRAPHY

Chakravarty, S., D.L. Hofeldt, W. Eichinger, and H. Kraye, Application of an elastic lidar for simultaneous mapping aerosol concentration and measuring effective index of refraction, SPIE International Symposium on Aerospace/Defense Sensing and Control and Dual-Use Photonics, 17-21 April, 1995, Orlando FL., 1995.

Chakravarty, S., D.L. Hofeldt, W. Eichinger, and H. Kraye, Wide Area Remote Sensing of Air Quality: Impact of IVHS, ITS America, Fifth Annual Meeting, 15-17 March, 1995, Washington, D.C., 1995.

Cicero-Fernandez, P. and J. Long, Effects of Grades and Other Loads on On-Road Emissions of Hydrocarbons and Carbon Monoxide, J. Air & Waste Manage. Assoc., Vol 47, pp 898-904, 1997.

Hofeldt, D and B. Olson, Lidar Measurements of Particle Concentrations Near Roadways, OSA Conference on Optical Remote Sensing of the Atmosphere, Feb 10-14, 1997, Santa Fe, NM; OSA 1997 Technical Digest, series 5, OMD9-1to 9-3.

Seinfeld, John, Atmospheric Chemistry and Physics of Air Pollution, John Wiley and Sons, New York, NY, 1986.

Sturm, P., R. Almbauer, C. Sudy, and K., Application of Computational Methods for the Determination of Traffic Emissions, J. Air & Waste Manage. Assoc., Vol 47, pp 1204-1210, 1997.

Sutton, O.G., Micrometeorology, McGraw-Hill Book, Co, New York, NY, 1953.

US Environmental Protection Agency, National Vehicle and Fuel Emissions Inventory, National Vehicle and Fuel Emissions Laboratory, April, 1997.

APPENDIX A

DESCRIPTION OF DATA COLLECTED

The following table is a list of all of the lidar data files collected during the experiment. Each file represents the particulate concentration in a two or three dimensional piece of the atmosphere. Each of the graphs of lidar data shown in this report are portions of these files.

The files are sorted by date and time. Listed is the name of the file, the size of the file, and the date and time at which the data were taken. For a vertical scan, the azimuth and elevation start and end angles are given as well as the incremental angle moved during the scan. For a horizontal scan, the elevation and azimuthal start and end angles are given as well as the incremental angle moved during the scan. The number of laser pulses averaged along each line of sight is given (in general, more averaged pulses correlates to longer range). Lastly a comment is included in the file that gives an indication of the area or object examined by the scan.

24 October 1995

24oct95\24OCT001.2D FileSize = 227224 10/24/1995 11:9
Elevation: 0.75 to 6.00 increment: 0.20 azimuth: 180.00 shots: 50
Looking Westward over the west bound lanes

24oct95\24OCT002.2D FileSize = 227224 10/24/1995 11:12
Elevation: 0.75 to 6.00 increment: 0.20 azimuth: 177.70 shots: 50
Looking Westward over the east bound lanes

24oct95\24OCT003.2D FileSize = 992296 10/24/1995 11:13
Elevation: 0.75 to 60.00 increment: 0.50 azimuth: 177.70 shots: 40
Looking Westward over the east bound lanes

24oct95\24OCT004.2D FileSize = 227224 10/24/1995 11:15
Elevation: 0.75 to 6.00 increment: 0.20 azimuth: 175.70 shots: 50
Looking Westward around the corner, over the trees

24oct95\24OCT006.2D FileSize = 260488 10/24/1995 11:17
Elevation: -1.50 to 4.50 increment: 0.20 azimuth: 10.00 shots: 50
Looking Eastward over the west bound lanes

24oct95\24OCT007.2D FileSize = 2056744 10/24/1995 11:18
Elevation: -1.50 to 60.00 increment: 0.25 azimuth: 11.50 shots: 40
Looking Eastward over the east bound lanes

24oct95\24OCT008.2D FileSize = 260488 10/24/1995 11:22
Elevation: -2.00 to 4.00 increment: 0.20 azimuth: 15.75 shots: 50
Looking Eastward over the hillside

THERE ARE 70 MORE PAGES OF LISTINGS

*** A complete listing of the files taken may be obtained from Santa Fe Technologies.***
*** They have been omitted here for brevity. ***

APPENDIX B

SITE DESCRIPTIONS

Three different vantage points for siting the lidars were used along critical sections of I-80 where a baseline measurement could be performed prior to the implementation of IMS. All of the sites were selected on the basis of a study conducted by NJDOT of the number of incidents occurring along I80. The first two sites were selected because they were in identified high accident areas in the eastern portion of the interstate. However, because of flight restrictions due to the proximity of Newark Airport to the south, the HNTB aircraft could not survey the eastern portion of I80 and thus the vehicle monitors also did not survey the eastern half of the interstate. This was identified as a problem on Wednesday, after the airplane started flying, and after setting up at the second site. The lidar and associated monitors were then moved to site three in the region where traffic monitoring was also conducted. All of the sites were selected with the knowledge and guidance of personnel from NJDOT.

* **Site #1:** Highway 80 behind the barriers along the highway near milemarker 62. This site was selected because it was identified as a high accident zone and had good fields of view along the highway in both directions. The site was a construction zone and thus had a series of barriers that formed a protected area in the middle of the highway. Setup was accomplished on Sunday 22 October, Data collection started 0700 23 October. The lidar was moved on the evening of Monday 23 October because the barriers that formed the protected area were removed the following day.

Figure B1: A photograph of the section of I80 designated as Lidar Site #1 looking east. The lidar was located between the east and west-bound lanes in a construction area just behind the photographer.

CO Monitors:

* #1648 & #1630 mounted on post #PO2121, near westbound lane, west of overpass.
* #1619 & #1635 mounted on an unnumbered post at the side of the road, 0.45 miles west of site 1.
* #1643 & #1650 mounted on the flux monitor tower immediately west of lidar van inside the barriers between the east and west bound lanes.

The CO Monitors were removed approximately 1755 hrs and the tower was removed at 1820 hrs on the 23rd of October..

* **Site #2:** Lidar was also sited in a construction site that was located between the east and west-bound lanes directly above the point where Hwy 17 goes under I80. This general location was selected because it is in the area of the highest incident occurrence. Data collection started 1130 hrs 24 October.

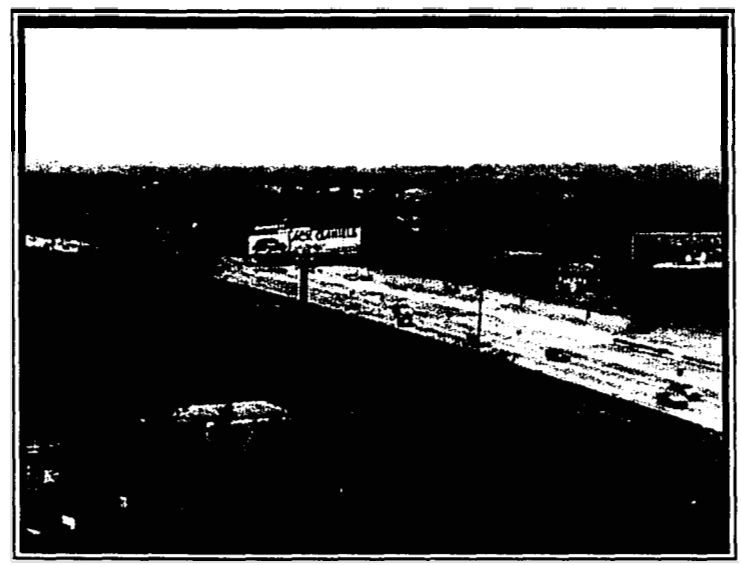

Figure B2: A photograph of the section of I80 designated as Lidar Site #2. The lidar was located between the east and west-bound lanes in a construction area just behind the sign in the center of the photograph.

This site was abandoned on the evening of 24 October because it was discovered that the site was east of the farthest point east that HNTB collected traffic data. Thus no traffic or incident data are available for this site from HNTB.

The tower and CO monitors were set up at 0750 hours on the 24th.

CO Monitors:

* #1648 & #1630 were mounted on an unnumbered post at the side of the road near the westbound lanes, 0.3 miles west of Lidar Site #2.

* #1619 & #1635 mounted on the underpass approximately 350 meters west of Lidar Site #2.

* #1643 & #1650 mounted on the flux monitor tower immediately west of lidar van in the area between the east and west bound lanes.

The CO Monitors were removed at approximately 1830 hrs, and the tower taken down at 1920 hrs.

* **Site #3:** The lidar was located on top of the Prime Business Building next to the Radisson Hotel at 40° 53.413' N 74° 16.189' W. Data collection was begun at 0930, 26 October.

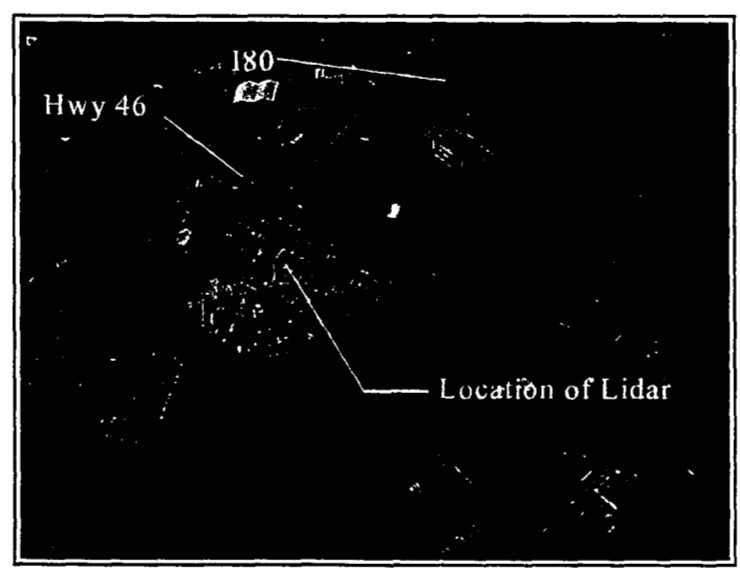

Figure B3: An aerial photograph of Lidar Site #3. The lidar was located on top of the building shown. I80 is the highway in the upper right hand of the picture. Hwy 46 extends from upper left to lower right.

All CO Monitors were recalibrated on the morning of 25 October. The locations of the monitors were:

Monitors #1663 and #1630, at the side of the road, at mile marker 54, 40° 53.829' N and 74° 13.589' W.

Monitors #1635 and #1619, at the side of the road, at mile marker 51 at 40° 53.610' N and 74° 18.029' W

Monitors #1648 and #1634, at the side of the road, approximately 3/10 mile west of the tower at 40° 53.667' N and 74°16.231' W

The tower was set up at 1145 26 October at 40° 53.660' N and 74° 15.954' W. The tower was placed at the east end of a small bridge in a grassy area between the east and west bound lanes. The CO monitors used on the tower were #1650 Bottom and #1643 Top. The tower and CO Monitors were removed on the morning of 31 October.

APPENDIX C

CASE STUDIES II AND III

LIDAR CASE STUDY - CASE II

The incident that will be examined here occurred on the afternoon of 28 October. The cause of the accident is unknown. Ambulances and fire trucks were observed from Lidar Site #3 moving along I80 to a spot approximately 1 mile to the east with traffic intermittently slowed or stopped. The incident and its effects appeared to last only a half hour. The lidar scans to be shown in this case study have been chosen to better demonstrate how the highway looks under normal conditions and how different they appear when an incident occurs.

Figures C1 and C2 show the highways to the east of Lidar Site #3 as they appeared prior to the incident. The area covered by the scans includes both I80 and Highway 46. Plumes from traffic can be seen in both figures. The area that in the middle of figure C2 is noteworthy for its lack of plumes. This should be compared to figure C4 which has several significant plumes in that area. Traffic on the highway is highly variable and intermittent when examined on short time scales. Thus it should be no surprise that the particulate concentration varies considerably as well. More intense traffic will produce plumes with higher concentration, all other factors being equal.

In case studies II and III we will continue to examine the general applicability of the criterion outlined in the first case study, which enables an incident to be identified by a particulate concentration over the highway that is a factor of three or more above the ambient air, or which has a concentration above the some threshold (in this study, about 10^8 (the units being arbitrary but consistent throughout all three case studies)). Concentrations approaching and over this threshold appear red in the following figures. All of the figures to follow have examples of plumes from the highways, entrances, and exits. One can identify the particular roads or highways associated with each plume by comparing to the map in figure 9. Examination of the plumes show that they range from ambient concentrations to concentrations approaching 50 percent above ambient indicating normal traffic levels and flow.

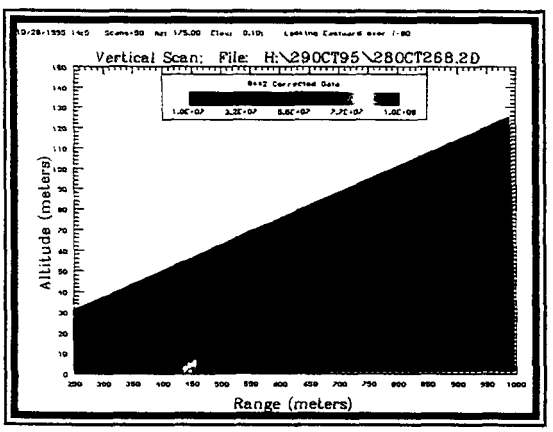

Figure C1: A lidar scan looking to the east from Lidar Site #3 prior to the incident. Time is 14:05.

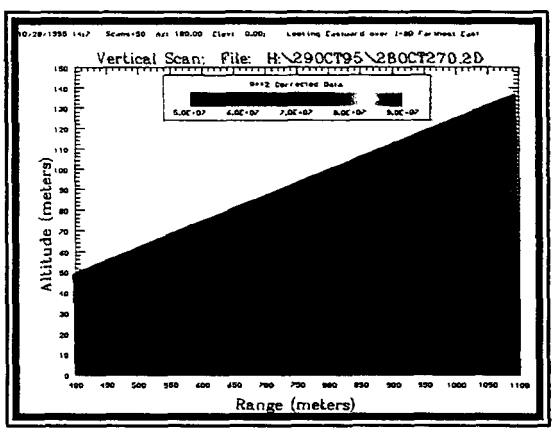

Figure C2: A lidar scan looking to the east from Lidar Site #3 prior to the incident. Time is 14:07.

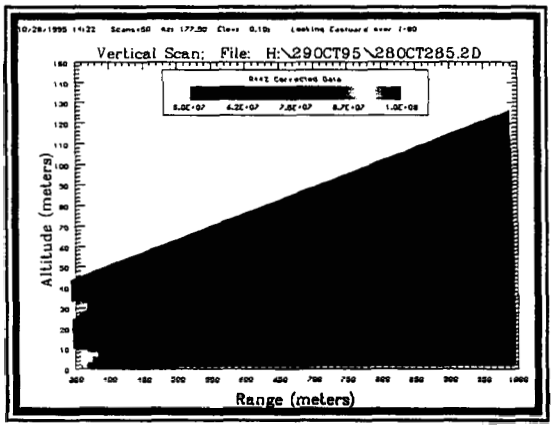

Figure C3: A lidar scan looking to the east from Lidar Site #3 during the incident. Time is 14:22.

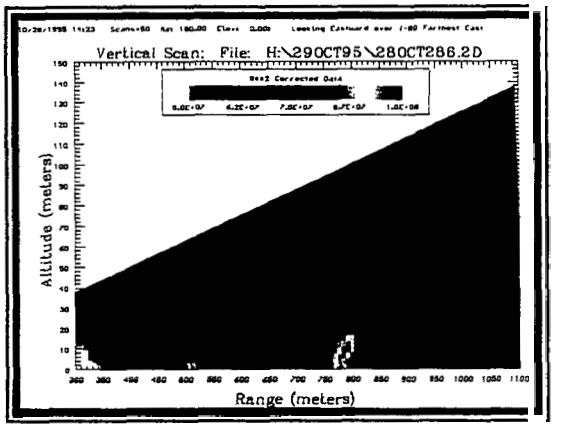

Figure C4: A lidar scan looking to the east from Lidar Site #3 during the incident. Time is 14:23.

Figures C3 and C4 are the first lidar scans during the incident. Figure C4 shows a plume at a distance of 775 meters that meets the criterion (concentration being greater than 10^8). Figures C5 and C6 show different portions of the same lidar scan. Figure C5 shows the nearer portion of the scan with relatively normal traffic. At a distance of 3500 meters, one can see two intense, close plumes which overlap. Of particular note is the contrast between the incident plumes here with the ambient air. Normal traffic plumes do not have differences of concentration this great over such short distances; they are normally much more diffuse.

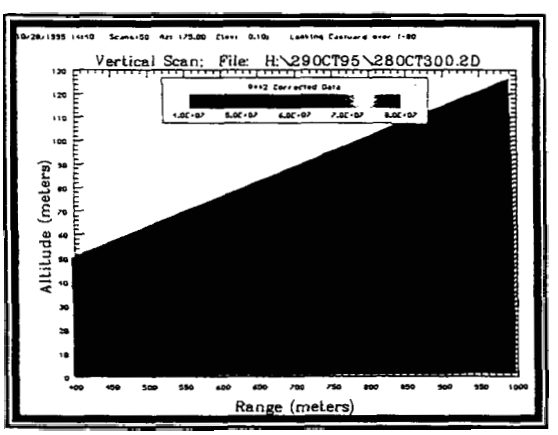

Figure C5: Lidar scan looking to the east from Lidar Site #3 during the incident. Time is 14:40.

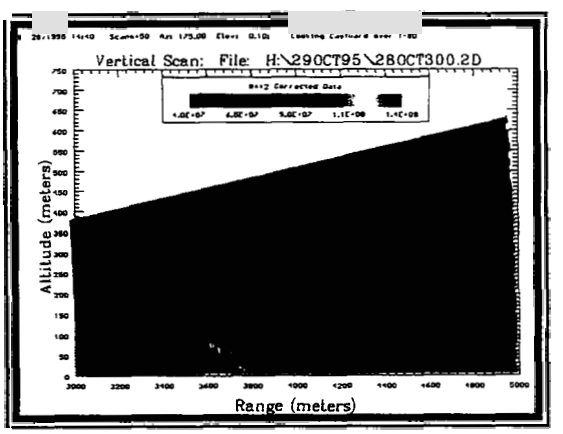

Figure C6: Lidar scan looking to the east from Lidar Site #3 during the incident. Time is 14:40.

Figure C7 is the last of the lidar scans that show incident levels of particulates, this time relatively close to the lidar. Again, there are plumes rising from other areas farther away that show normal traffic levels.

The remaining figures show examples of normal traffic from the 26th and 28th of October. Again, examination of the graphs show the same types of plumes for normal traffic, with similar concentration differences and texture. Figure C9 shows a scan that meets the criterion for an incident, but since it occurred over highway 46, no information is available on the traffic conditions there for that time.

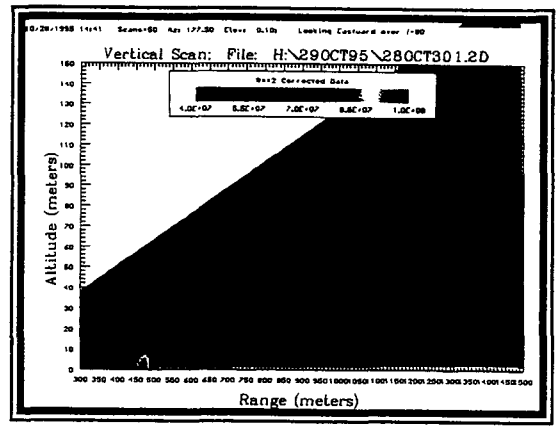

Figure C7: Lidar scan looking to the east from Lidar Site #3 during the incident. Time is 14:41.

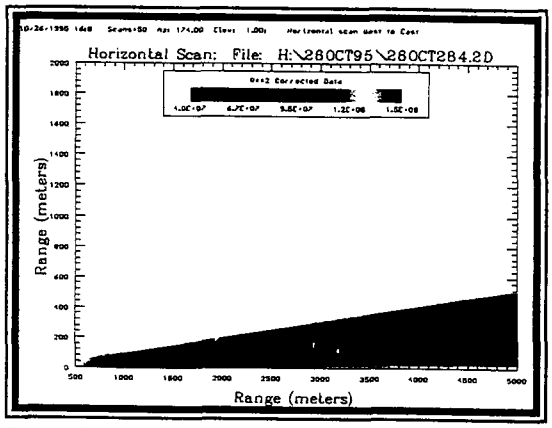

Figure C8: Lidar scan looking to the east from Lidar Site #3 during normal traffic. Time is 14:08.

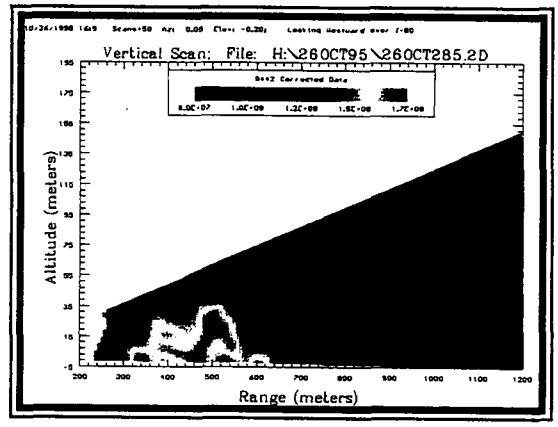

Figure C9: Lidar scan to the east from Lidar Site #3 during a possible incident. Time is 14:09.

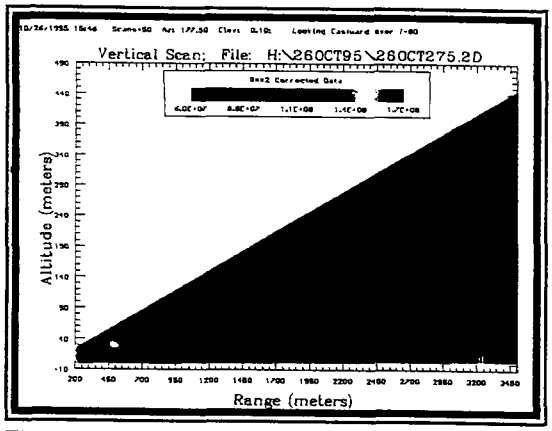

Figure C10: Lidar scan looking to the east from Lidar Site #3 during normal traffic. Time is 15:46.

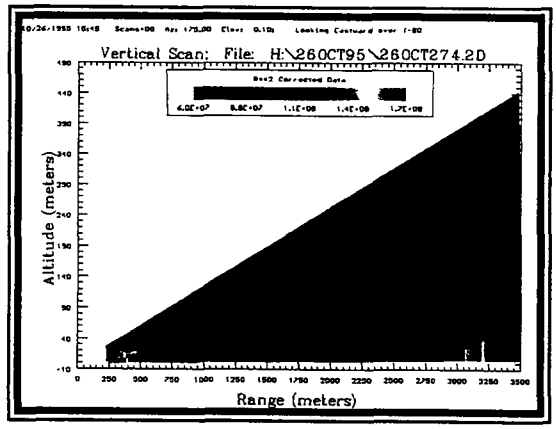

Figure C11: Lidar scan looking to the east from Lidar Site #3 during normal traffic. Time is 15:45.

Figures C12 and C13 are again lidar scans during normal traffic conditions, but have been chosen to illustrate two limitations of the lidar. When abnormally high concentration or absorptive conditions exist close to the lidar, they may attenuate the lidar beam. This results in a region with abnormally low concentrations (as can be seen in figure C12 from about 2000 to 2500 meters). This does not prohibit the identification of highway plumes or incidents (a plume at 2600 meters is clearly visible), but does mean that for conditions in which the laser beam is strongly attenuated, this type of lidar data cannot be used as a quantitative measure of particulate density. The use of a reliable inversion method will correct this problem and enable quantitative measurements under all types of conditions.

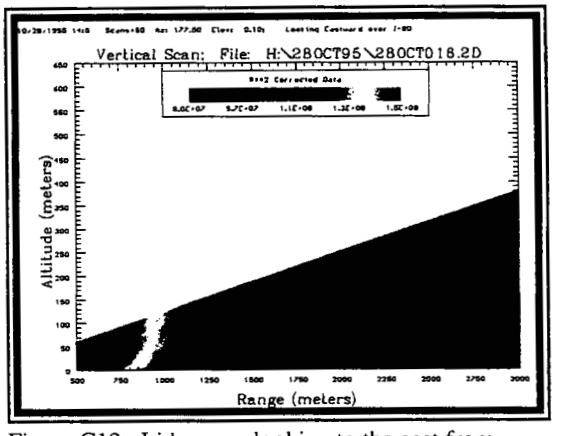

Figure C12: Lidar scan looking to the east from Lidar Site #3 during normal traffic. Time is 14:05.

Lidars also have a minimum range at which they normally operate. This is because, in the near field, the telescope does not "see" all of the laser beam. Normal operation of the lidar commences when the telescope field of view completely encompasses the laser beam. The minimum range is generally about 100 to 300 meters and depends upon the details of the lidar design as well as the details of the alignment of the laser beam. This effect can be seen in many of the figures throughout the three cases. Again, this effect prohibits quantitative measurement of concentrations, but does not prohibit qualitative comparisons within the excluded region. The effect can be mitigated through the application of an analytical algorithm which compensates for the laser - telescope alignment. In most cases, measurements to long range by the lidar are desired more than information in the near field. Should short range measurements be desired, they can be reliably obtained by shortening the length of the periscope with the result of some penalty on the maximum distance that can be examined.

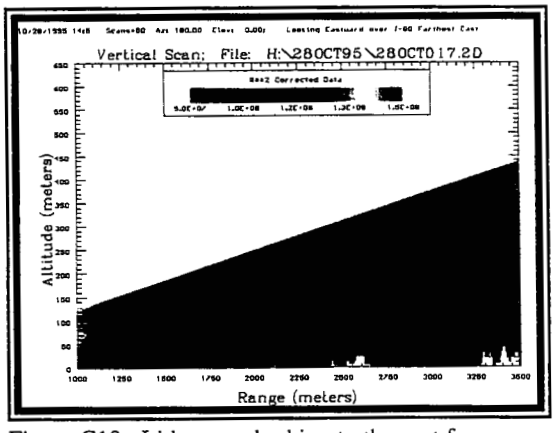

Figure C13: Lidar scan looking to the east from Lidar Site #3 during normal traffic. Time is 14:05.

Each of the lidar scans shown in the second case study confirm the general conclusions reached in the first. Specifically, that the concentration levels found during incidents are much higher than those normally found over highways, and that they can be reliably identified. Because relatively few incidents were identified during the campaign (only four were identified by the lidar team and none were reported by HNTB by date and time), there are a limited number of examples for incident level concentrations.

LIDAR STUDY - CASE III

The plots of lidar data that are again graphical depictions of the intensity of the lidar return signal in two dimensions, corrected for range and average attenuation effects. The data shown here are from an incident during foggy/limited visibility conditions and in which some of the limitations of lidar data are

shown. This case was selected to demonstrate that even under relatively adverse conditions, the lidar can still identify and locate traffic incidents. The area examined in this case study is outside the area monitored by HNTB, but in a region identified by NJDOT as a high incident area and of great interest.

The day of the incident was 24 October, 1994. The day was foggy and overcast. At the time of the incident, the fog/low cloud layer was 200-300 meters above the surface. In the lidar scan shown in figure C14, one can see the intense cloud layer and often "fingers" extending from the cloud to the surface. These fingers can be mistaken for intense sources. The lidar itself cannot distinguish between particles caused by fog and particles caused by traffic. Thus the situation to be described constitutes a severe test of the system's ability to operate under relatively adverse conditions. The origin and shape of the fingers is different from sources on the surface and these clues allow one to successfully identify problem areas. The fingers due to atmospheric water-vapor are connected to the clouds above and not the surface. They also often lack an intense central portion that true plumes from highways have.

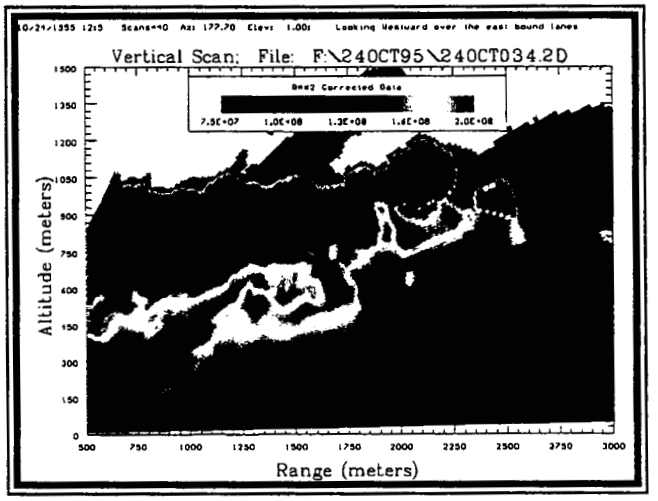

Figure C14: Showing a low level cloud/fog layer.

The incident which occurred was caused by several workers with a "cherry-picker" that were trimming trees and underbrush near the side of the road. They had blocked traffic in one or more of the east-bound lanes about a kilometer to the west of the Lidar Site #2. The workers were generally traveling from east to west along the highway causing traffic to be occasionally backed up along I-80 to the west. An on-ramp compounded the backup with traffic from the on-ramp attempting to merge with the flow.

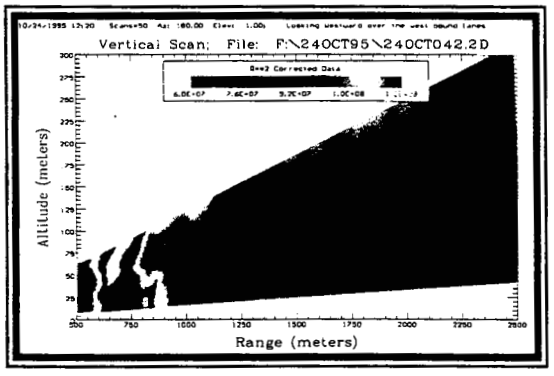

Figure C15: Lidar scan at 1220 hours looking west.

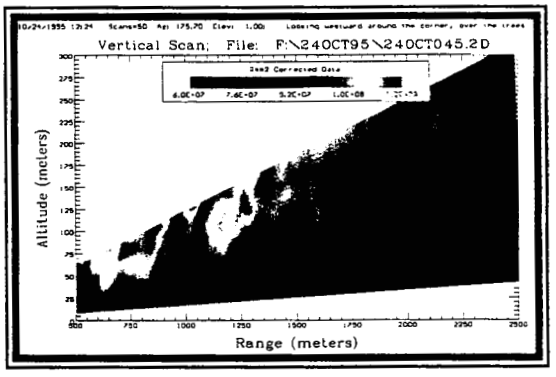

Figure C16: Lidar scan at 1224 hours, looking west.

The lidar team first identified the cause of the incident at about 1300 hours and confirmed the completion of

are shown. They are 2.5 degrees apart and show slightly different portions of the highway. It is important also to note that for the incident here, the traffic was backed up and slowed, but not actually observed to stop.

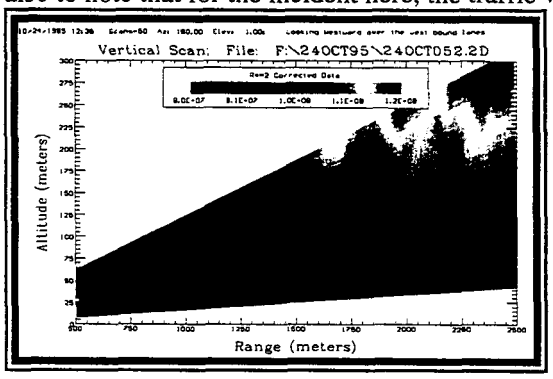

Figure C17: Lidar scan at 1235 hours, looking west.

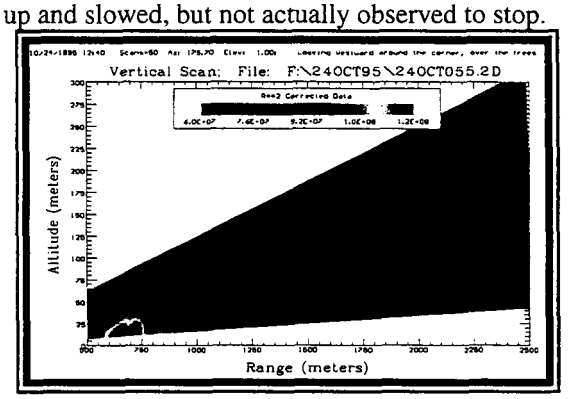

Figure C18: Lidar scan at 1240 hours, looking west.

At about 1230 hours the workmen appear to have moved their equipment approximately 700 meters farther down the highway to the west. The highest concentrations were 600-700 meters from the lidar (see figure C18) and are now near 1100 meters.

Figure C19: Lidar scan at 1251 hours, looking west.

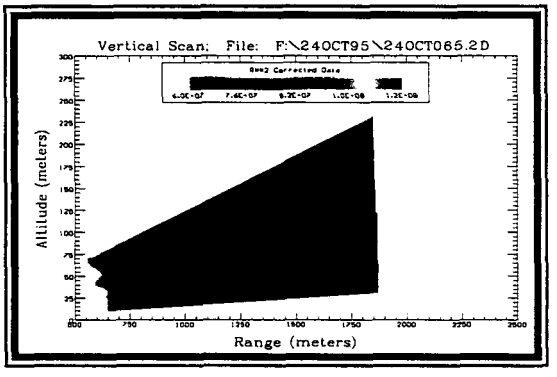

Figure C20: Lidar scan at 1255 hours, looking west.

At time the traffic becomes relatively free-flowing so that while one can observe higher particulate concentrations over the highway (for example 1400 meters figure C21, or 800 and 1200 meters on figures C20, C23, or C24), they are not sufficiently high to be called an incident by the definition described previously. One should note the intense concentrations in figure C22 that are located above the highway, but not connected to it. These are "fingers" of moisture rich air moving downwards from the fog layer above. These should not be confused with an incident. In examining the figure C22, one can see that these intense regions do not intersect the ground and thus do not have their origin at the surface.

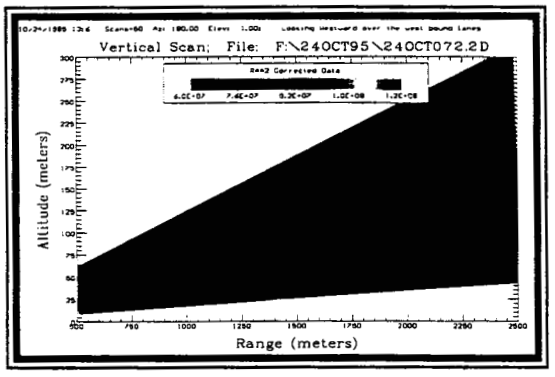

Figure C21: Lidar scan at 1306 hours, looking west.

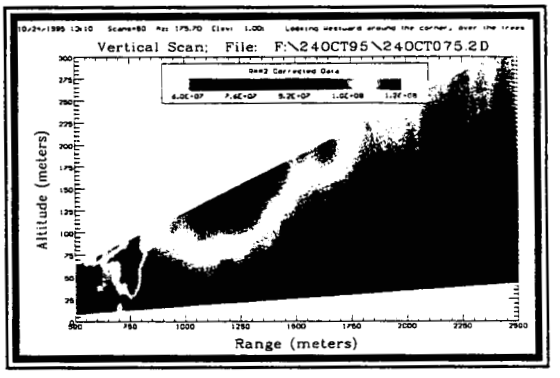

Figure C22: Lidar scan at 1310 hours, looking west.

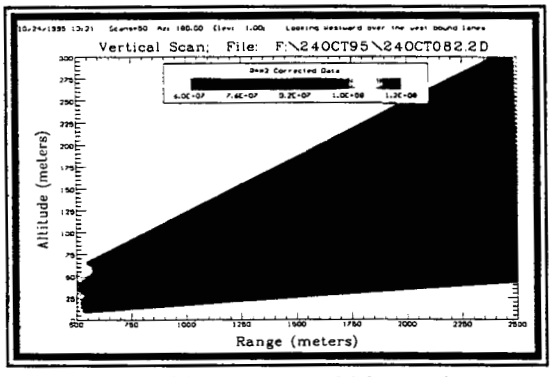

Figure C23: Lidar scan at 1321 hours, looking west.

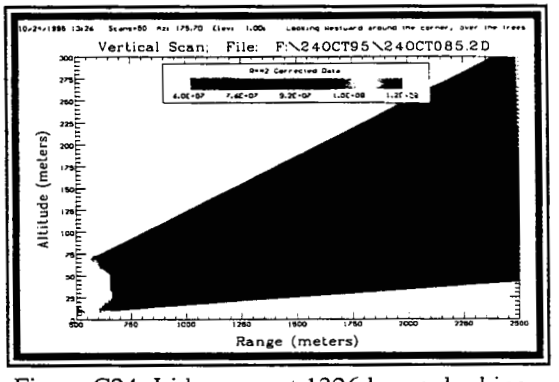

Figure C24: Lidar scan at 1326 hours, looking west.

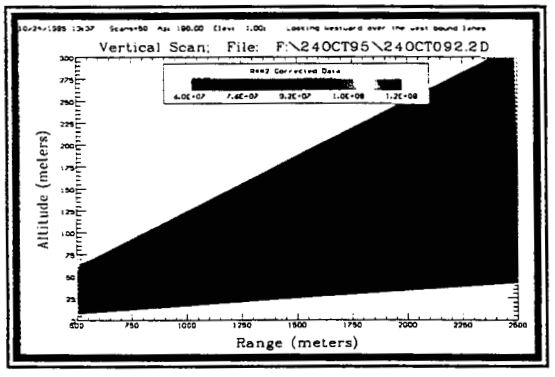

Figure C25: Lidar scan at 1337 hours, looking west.

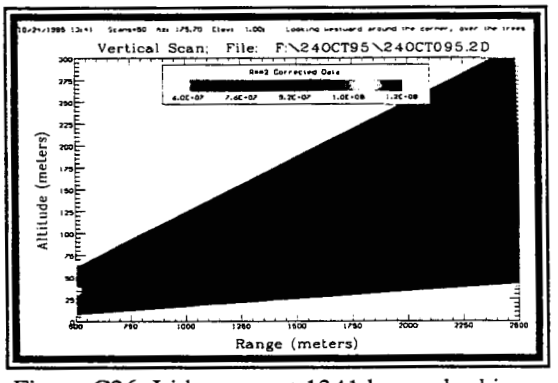

Figure C26: Lidar scan at 1341 hours, looking west.

At this time the workers move their equipment further to the west and cause traffic slowdown along the highway between 1250 and 1700 meters (see figures C27 or C28 for example). They work at this location

for about 15 minutes and leave the area. Once can see remnants of the traffic plume in figure C27, but for the most part the traffic is flowing freely again and the particulate concentrations are back to near normal for over the highway.

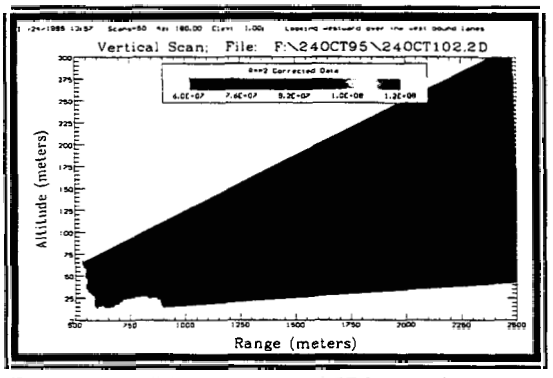

Figure C27: Lidar scan at 1357 hours, looking west.

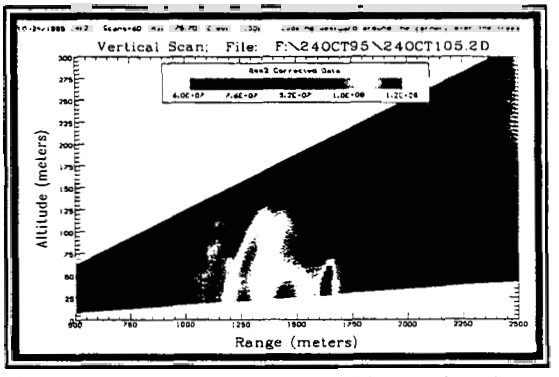

Figure C28: Lidar scan at 1402 hours, looking west.

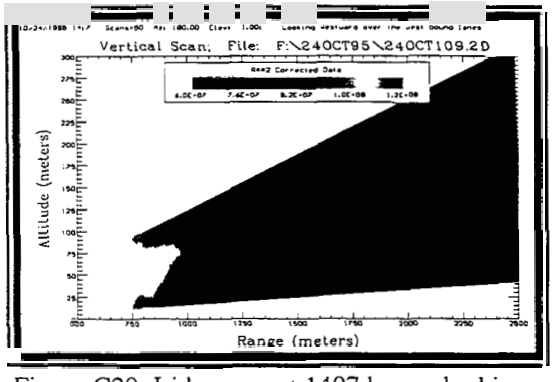

Figure C29: Lidar scan at 1407 hours, looking west.

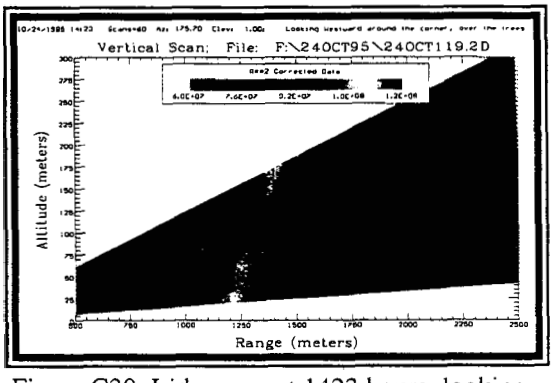

Figure C30: Lidar scan at 1423 hours, looking west.

To show the contrast between the incident area and other, more free-flowing traffic areas, the next set of six figures shows the area to the east of Lidar Site #2. The backgrounds of the following figures are similar to those in the scans above. For example, the foggy period from about 1245 to 1330 can be seen in figure C35, just as it can be seen in figures C25 through C30 above. However, one doesn't see the intense plumes rising from the surface and with the exception of a small plume at 650 meters in figure C28 and a weak plume at 1300 meters in figure C28, there are no surface features at all. The comparison between an incident with traffic back up as shown in figure C28 and a free flowing traffic as seen in figures C29 or C30 is dramatic and clear.

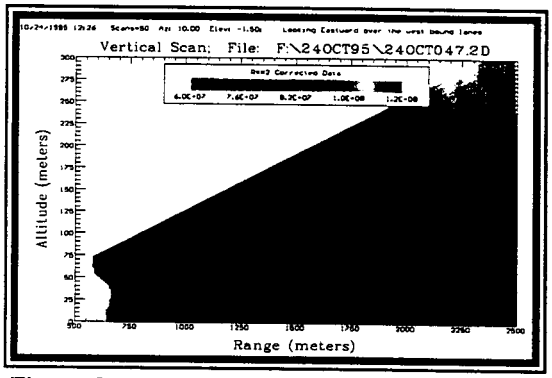

Figure C31: Lidar scan at 1226 hours, looking east.

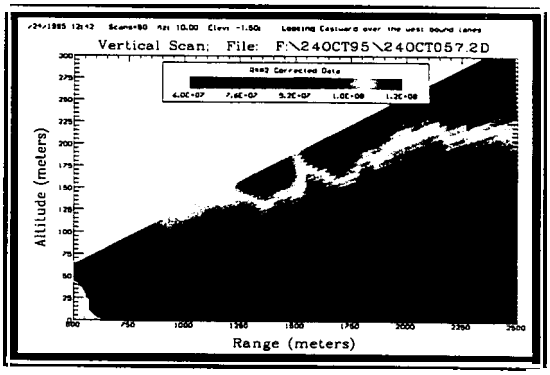

Figure C32: Lidar scan at 1242 hours, looking east.

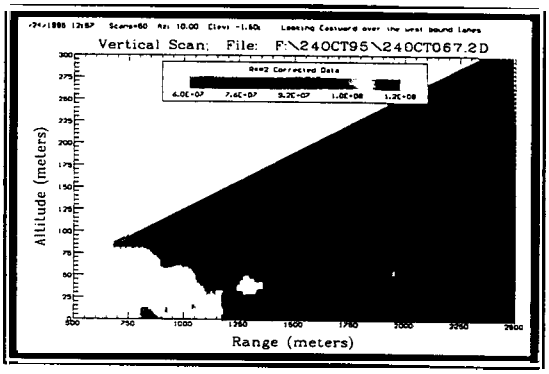

Figure C33: Lidar scan at 1257 hours, looking east.

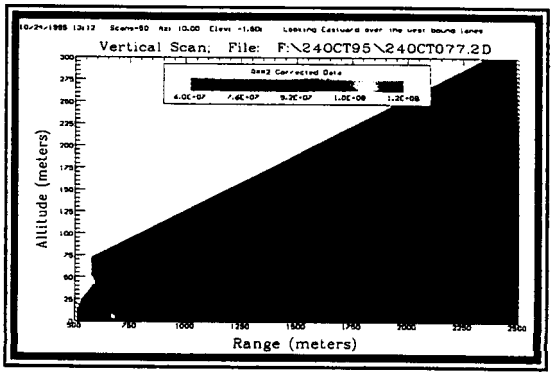

Figure C35: Lidar scan at 1312 hours, looking east.

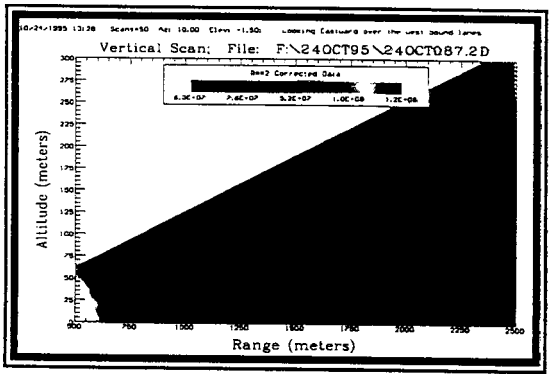

Figure C36: Lidar scan at 1328 hours, looking east.

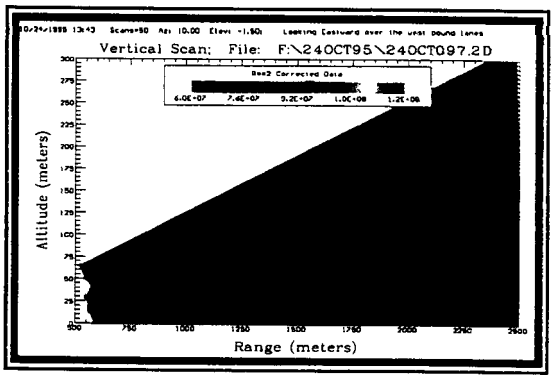

Figure C38: Lidar scan at 1343 hours, looking east.

APPENDIX D

ELASTIC LIDAR DESCRIPTION

Lidar stands for LIght Detection and Ranging. The lidar systems are laser based systems that operate on the similar principles as radar (RAdio Detection and Ranging). In the case of lidar, a laser beam scans through the atmosphere over a desired range of directions and elevations. Light from the beam is scattered from molecules and particulates in the atmosphere. A portion of the light is scattered back towards the lidar system, is collected by a telescope and is measured with a photo-detector. The signal contains information on the concentration of various atmospheric constituents as a function of distance from the source. The signal is digitized and analyzed by a computer to create a detailed image of the concentrations within the scanned region. The computer runs preprogrammed scan routines and processes raw lidar information via the E-LASTIC© and E-VIEW© software routines. On-site graphics are presented in a color display of spatial concentrations.

Figure D1: The lidar in operation on the top of the Prime Building, Lidar Site #3, looking towards the east. Visible are the laser power supply (bottom box), the stepper motor power supply (middle box), and the telescope with the laser and periscope attached on top. The computer and operators electronics are below.

The miniature particulate, elastic lidar is a small, scanning lidar which uses elastic backscattering (elastic refers to the fact that the light coming back is the same wavelength as the light sent out by the laser) to determine the distribution and properties of atmospheric particulates. The lidar operates by emitting a short (≈ 10 ns long) pulse of infrared laser light into the atmosphere. Particulates and, to a limited extent, molecules interact with the pulse and scatter light back toward the lidar. The amount of returning light collected by the telescope is proportional to the particulate content of the air and the amount of atmospheric attenuation. The system is capable of operation day and night through the use of a 3-nm wide interference filter, well-blocked in the visible and near infrared, with a peak transmission of 52 percent.

The lidar is contained in three carrying cases and a portable external electronics crate. The first case contains the laser power supply and chiller. The second case contains the scanner motor power supply and controller as well as the power supply for the detector. The third case contains the telescope and its mount with scanning motors built in (see Figure). A portable computer to control the system and take the data completes the major components of the lidar. The computer controls the external electronic system using high speed data transfer capabilities. The azimuth and elevation motors are controlled through a card on the PC bus which confers a rapid

scanning capability to the system.

A Nd:YAG laser operating at 1.064 microns is used as the laser source. The laser is attached directly to the top of a 21 cm, f/10, Cassegrain telescope. The laser beam is emitted parallel to the telescope after going through a periscope, so that the effective exit aperture is 41 cm from the center of the telescope. The periscope simplifies alignment, and also increases the distance at which the laser beam overlaps the telescope FOV. This separation decreases the chance of near-field detector overloading, and decreases the dynamic range required of the analog-to-digital conversion system. The telescope-laser system is able to turn rapidly through 180 degrees horizontally and 90 degrees vertically using motors incorporated into the telescope mount.

Behind the telescope, the light passes through the interference filter and a lens system which focuses the light on a 3-mm diameter, IR-enhanced silicon avalanche photodiode (APD). The signal is amplified as part of the detector system and fed to a 12 bit digitizer also on the PC data bus. Two detectors mounted in the periscope sample the outgoing laser pulse and produce signals which are used to correct for pulse-to-pulse variations in the laser energy and also serve as a timing marker to start the digitization process. Pulse averaging is used to increase the useful range of the system. A series of pulses are summed to make a single scan. A number of scans are used to build up a two-dimensional map of relative atmospheric particulate concentrations.

The determination of backscatter and extinction information from elastic lidars is a classic inverse problem in remote sensing [Hinkley 1976, Measures 1984]. The lidar equation is written as:

$$P(r) = \frac{C_1 E \beta(r) \exp[-2\int_0^r \alpha(r')dr']}{r^2} \tag{1}$$

where P(r) is the received signal strength, r is the range from the lidar, E is the laser energy per pulse, $\beta(r)$ is the backscatter coefficient for 180 degrees at the laser wavelength, $\alpha(r)$ is the attenuation coefficient for the laser wavelength, and C_1 is a system coefficient which takes into account the effective area of the telescope, the transmission efficiency of the optical train, and the detector quantum efficiency. The backscatter and extinction coefficients at each range are not fully quantified by a single wavelength system. Thus, a unique solution to (1) is not available for the general case and some assumptions must be made to reduce the number of independent variables. The most common assumption is the "Klett" assumption that the extinction to backscatter ratio is constant, or alternately, that the relationship is a power law, $\beta = C_2\sigma^k$, where C_2 is a constant. The value of the attenuation coefficient at the farthest usable range must be measured or assumed. [Klett, 1981; Klett, 1985]. The value of the attenuation coefficient at each range (r) can be found by working backwards from the reference position using:

$$\sigma(r) = \frac{[P(r)r^2]^{1/k}}{P(r_e)r_e^2/\sigma_e + \frac{2}{k}\int_r^{r_e}[P(x)x^2]^{1/k}dx} \tag{2}$$

where the subscript e specifies the values at the farthest range. There are several variants on this scheme [e.g. Ferguson, 1983; Mulders, 1984] to improve convergence of the inversion to the "correct" solution.

Normally the lidar is programmed for a series of scans which depend on the area to be scanned. During each cycle, the lidar will make a series of horizontal scans which cover the area and vertical scans which provide an in-depth look at specific areas. These areas are chosen because they are either potential "hot" spots or should be typical of a region. Three dimensional scans are also done, especially during an event. The operators can quickly change from one scan pattern to another or adjust the number and type of scans to accommodate the particular circumstances. A series of these scans is a cycle. A cycle will take anywhere from 20 minutes to 45 minutes to complete depending on the size of the area to be examined and the number of specific sites to be examined. These cycles are repeated throughout the day and normally disrupted only for identified incidents.

Figure D2: Lidar operators station with the lidar above. The operator controls the data collection computer and has a number of instruments to help him monitor the progress of the data collection. These include a two-dimensional real time display of the lidar data, a video camera showing where the lidar is currently pointing, and an oscilloscope to show the individual lidar signals.

REFERENCES

Ferguson, J.A. and D.H. Stephens, 1983: Algorithm for inverting lidar returns, *Appl. Opt.*, **22**, 3673-3674.

Hinkley, E.D., 1976: Editor, Laser Monitoring of the Atmosphere, Springer-Verlag, New York, 378 pp.

Klett, J.D., 1985: Lidar inversion with variable backscatter/extinction ratios., *Appl. Opt.*, **24**, 1609-1624.

Klett, J.D., 1981: Stable analytical inversion solution for processing lidar returns., *Appl. Opt.*, **20**, 1638-1647.

Measures, R.M., 1984: Laser Remote Sensing, Wiley Interscience, New York, 510 pp.

Mulders, J.M., 1984: Algorithm for inverting lidar returns : Comment, Appl. Opt., **23**, 2855-2856.

APPENDIX E

CO FLUX DETERMINATION

Heat, Momentum, and Carbon Monoxide Fluxes from Monin Obukov Similarity Theory using Fixed Measurements

Comparisons of the concentrations of particulates or chemical pollutants is normally not sufficient to draw conclusions with respect to whether a particular mitigation strategy was successful or not. This is because the concentration of a pollutant at a given location is a function not only of the amount of that pollutant being added to the atmosphere, but also of the state of the atmosphere, specifically, the ability of the atmosphere to locally disperse the pollutant. This ability is, in turn, a function of the wind speed and stability of the atmosphere (which is related to the change in temperature with altitude). Thus for a given, constant, release rate, nearly any concentration could be measured depending on the atmospheric conditions. Thus a measurement of concentration alone gives no information about the amount of the pollutant being released into the atmosphere.

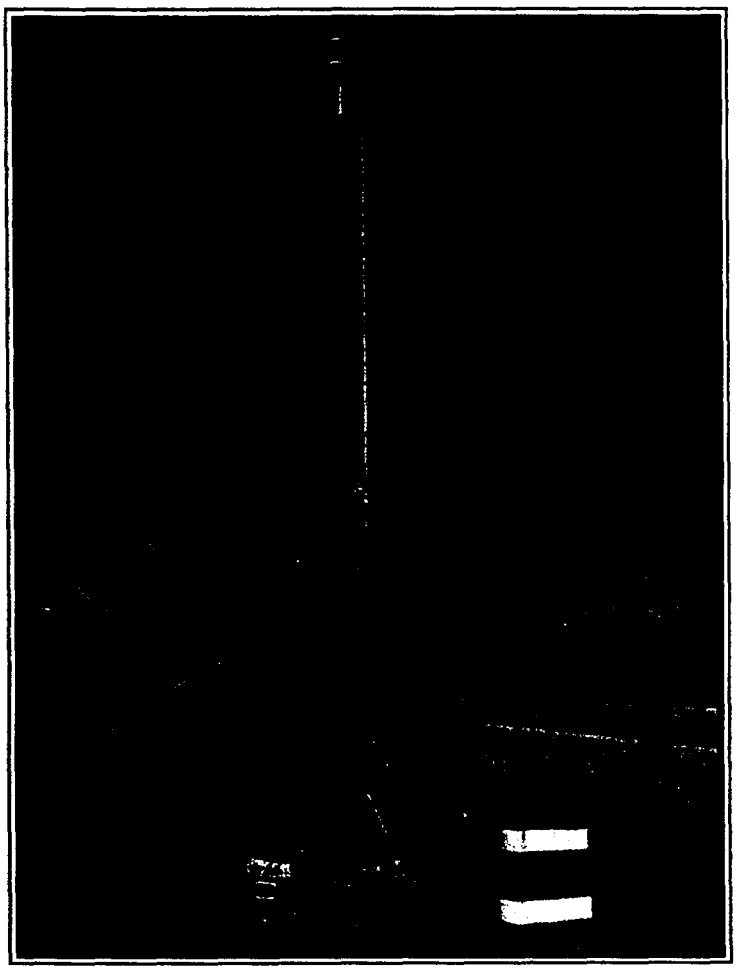

Figure E1: The setup used to determine the emission rates of carbon monoxide along Interstate 80 in New Jersey. At the top of the tower is the 3D sonic anemometer, at various heights are temperature and CO sensors, and a cooler at the base which contains the battery and data logging equipment.

To accurately access the efficacy of a particular mitigation method, information must be obtained on the emission rate of the pollutants of interest. Surface emission rates (or fluxes) of water and heat are routinely obtained by micrometeorologists using a number of techniques. The Monin-Obukov similarity theory method (MOM) [Brutsaert, 1984] is particularly useful in that it allows one to extend measurements made of one species to another through the concept of similarity. Similarity refers to the idea that the

atmosphere transports all trace chemical species in a "similar" manner. This implies that changes in concentration with height of each species are related to their relative emission rates. Thus a measurement of the emission rate of one can be extended to other chemical species. Here, direct measurements were made of the sensible heat flux (the warming of the air from energy deposited at the surface by the sun) as well at measurements of temperature and carbon monoxide at two heights above the ground.

With this theory, the relationships between the surface emission rates and the concentrations (or temperatures) at heights, z_1 and z_2, within the inner region are given by:

$$T(z_1) - T(z_2) = \frac{H}{C_p k u_* \rho}\left[\ln\left(\frac{z_2 - d_o}{z_1 - d_0}\right) + \psi_h\left(\frac{z_1 - d_o}{L}\right) - \psi_h\left(\frac{z_2 - d_o}{L}\right) \right] \quad (1)$$

$$U(z) = \frac{u_*}{k}\left[\ln\left(\frac{z - d_o}{z_{om}}\right) + \psi_m\left(\frac{z - d_o}{L}\right) \right] \quad (2)$$

The Monin-Obukhov length, L, is defined as:

$$L = -\frac{\rho u_*^3}{kg\left[\frac{H}{Tc_p}\right]} \quad (3)$$

where z_{0m} is the roughness length for momentum, Ψ_v and Ψ_h are the Monin-Obukhov similarity functions for water vapor, temperature and momentum, d_0 is the displacement height, ρ is the density of the air, Cp is the heat capacity of the air, H is the sensible heat flux, T(z) and u(z) are the temperature and wind velocity at height z, and u_* is the friction velocity (a measure of the ability of the atmosphere to mix trace constituents vertically) [Brutsaert, 1984], k is the von Karman constant, equal to 0.40, and g is the acceleration due to gravity. The roughness length, z_0, and d_0 are a free parameters to be calculated based upon the local conditions and can be estimated from the sensible heat flux which is measured by the three-dimensional sonic anemometer.

The three-dimensional sonic anemometer makes high speed, direct measurements of the wind velocity and speed of sound in three dimensions. From this, the friction velocity, u_*, temperature, T, wind velocity, u, and sensible heat flux, H can be determined. When combined with temperature measurements at two heights above the ground, all of the parameters in equations 1 through 3 can be determined.

In a manner similar to that for heat (equation 1), a relationship for the carbon monoxide flux can be written as:

$$CO(z_1) - CO(z_2) = \frac{COFlux}{k u_* \rho}\left[\ln\left(\frac{z_2 - d_o}{z_1 - d_0}\right) - \psi_v\left(\frac{z_2 - d_o}{L}\right) + \psi_v\left(\frac{z_1 - d_o}{L}\right) \right] \quad (4)$$

Where CO(z) is the concentration of carbon monoxide in gm-CO/kg-air at a height of z. For the case where the carbon monoxide measurements are made at the same height as the temperature measurements, this reduces to a simple expression:

$$COFlux = \frac{H\ [\ CO(z_1) - CO(z_2)\ ]}{C_p\ [\ T(z_1) - T(z_2)\ ]} \tag{5}$$

where H can be independently determined from the three-dimensional sonic anemometer at the top of the tower.

The experimental set up shown in figure E1 was operated over a period of days in a narrow grassy area between the east and west bound lanes of Interstate 80 in northern New Jersey. The system was set up each morning and taken down at night to allow for recharging of the batteries that powered it and to preclude vandalism. Figure E2 shows the results of a calculation of the emission rate for carbon monoxide.

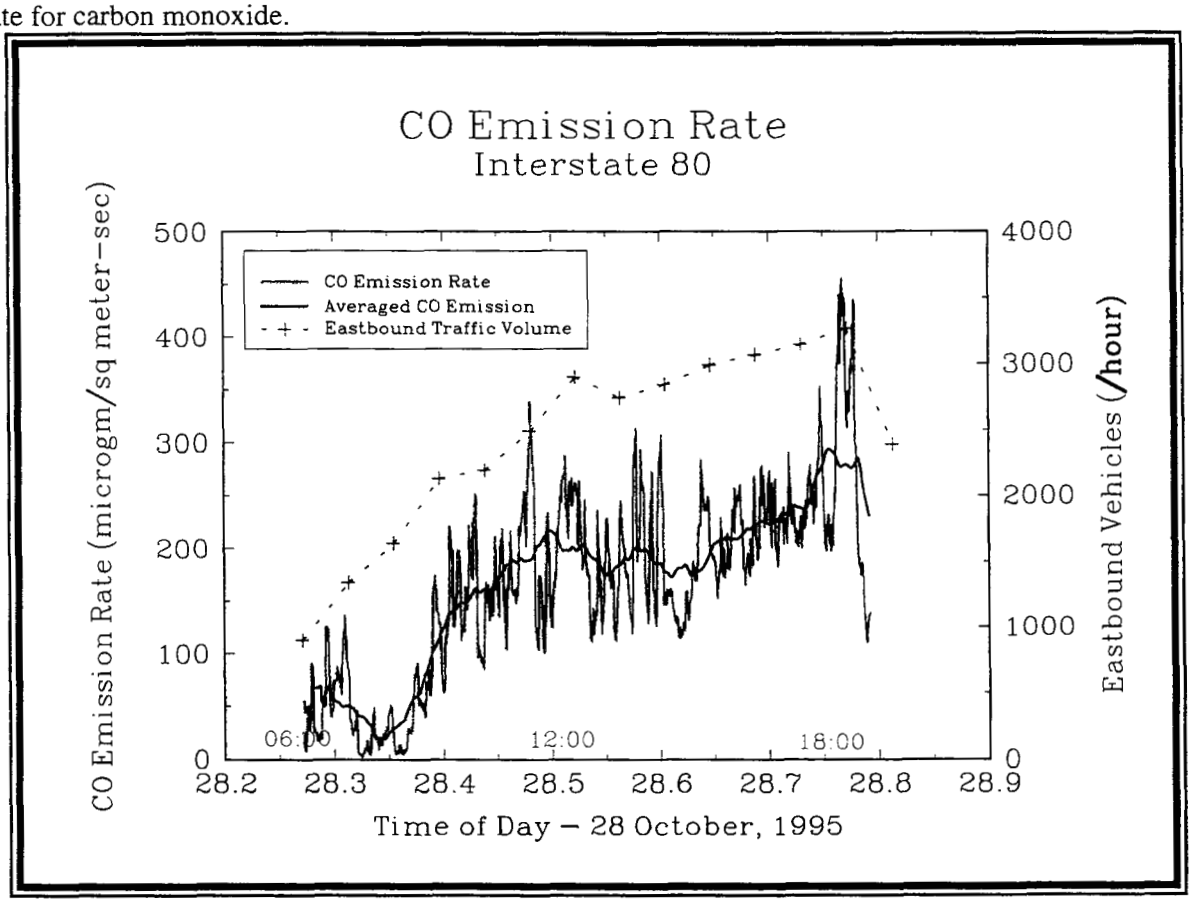

Figure E2: Measured CO emission rates for 28 October and the hourly traffic volume on the eastbound lanes of I80. The dark solid line is the smoothed emission rate.

The CO emission rates shown in figure above may be compared to estimates based upon the

emission rates of CO from an average vehicle and the traffic volume during the day of the measurements. For the day during which the CO measurements were made, traffic volume data near the experimental site is available for only the eastbound lanes (NJDOT control station at milemarker 54.72). We shall assume that the traffic volume in the westbound lanes is similar to the eastbound lanes. The emission rate of CO from an average vehicle is given by the National Vehicle and Fuel Emissions Laboratory of the EPA (EPA, 1997) as approximately 22 grams of carbon monoxide per mile for an "average" vehicle. Estimating the roadway (both directions and all lanes) as 50m, this results in an emission rate of about 275 $\mu g/(m^2$- vehicle/second). Thus a traffic count of about 6000 vehicles per hour (for both east and west bound lanes) would be expected to produce an emission rate of about 460 micrograms/m^2-s. The emission rates described by Cicero-Fernandez and Long [1997] and Sturm et al. [1997] range from 4 g/mile to about 8 g/mile. A value of 6 g/mile results in an emission rate of about 125 micrograms/m^2-s. The data presented here lie between these two extremes.

The emission rates at dawn and dusk appear to be anomalously high. Whether this is due to the abrupt change in weather conditions (very cold and damp) causing a change in the average CO emission by the vehicles, or whether the change in weather resulted in a change in the atmospheric stability that affects the measurements is not yet resolved.

The uncertainty in the CO flux measurement can be estimated using the expression below.

$$\frac{\delta CO\ Flux}{CO\ Flux} = \left[\left(\frac{\delta H}{H} \right)^2 + \left(\frac{\delta(CO_{z_1} - CO_{z_2})}{(CO_{z_1} - CO_{z_2})} \right)^2 + \left(\frac{\delta(T_{z_1} - T_{z_2})}{(T_{z_1} - T_{z_2})} \right)^2 \right]^{1/2} \tag{6}$$

The uncertainty in the measured values can be estimated in advance. Of the three terms, the uncertainty in the sensible heat flux is the most difficult to estimate. It is generally accepted that the accuracy of the sonic anemometer in estimating the sensible heat flux is between 5 and 10 percent. Given the resolution of the CO monitors as 50 ppb, the uncertainty in CO differences is on the order of 0.1 ppm or about 10 percent of a typical difference. Similarly, the resolution of the temperature sensor is given as 0.1 °C, making the uncertainty in temperature differences is on the order of 0.2 °C or about 10 percent of a typical temperature difference. Thus the overall uncertainty in the CO flux measurement is expected to be on the order of 15 percent.

There are some drawbacks to this method of measurement. While the derivation of equations 1 through 4 imply a source region of infinite extent, the source region along a highway is limited in size, with a strong directional dependance (the amount of highway surface differs depending on which direction one looks). Because the source region does not include the exact location of the sensor, there is a minimum height below which the lowest sensor cannot be placed. Because the size of the source region is limited, there also exists a height above which the highest sensor must not be placed. More modeling effort must be done to estimate these heights for various conditions.

Also implicit in the derivations is an assumption of horizontal homogeneity. This is often not true for highway situations, especially in the western part of the Interstate 80 corridor where the

interstate runs through many forested areas or is lined with trees. To some extent, this limitation is made up for by making a direct measurement of the sensible heat flux and relating the carbon monoxide flux to the relative gradients of temperature and carbon monoxide.

References

Brutsaert W., Evaporation Into the Atmosphere, Reidel Pub. Comp., Dordrecht, Holland, 1984.

Cicero-Fernandez, P. and J. Long, Effects of Grades and Other Loads on On-Road Emissions of Hydrocarbons and Carbon Monoxide, J. Air & Waste Manage. Assoc., Vol 47, pp 898-904, 1997.

Garratt, J.R., The Atmospheric Boundary Layer, Cambridge University Press, New York, 1992.

Kaimal, J. and J. Finnigan, Atmospheric Boundary Layer Flows, Oxford Univ. Press, New York, 1994.

Sturm, P., R. Almbauer, C. Sudy, and K., Application of Computational Methods for the Determination of Traffic Emissions, J. Air & Waste Manage. Assoc., Vol 47, pp 1204-1210, 1997.

US Environmental Protection Agency, National Vehicle and Fuel Emissions Inventory, National Vehicle and Fuel Emissions Laboratory, April, 1997.

APPENDIX F

NJDOT ACCIDENT DATA

10/23/95 through 10/30/95 Mileposts 42-60 of I80
sorted by location

control #	Milepost	Dir	Weather	Light	Date	Day	Time	Injury	Death
825905	42.63	W	C/D	DNDK	23 Oct	Mon	1800	0	1
787501	42.63	E	C/W	Day	30 Oct	Mon	0800	0	0
825878	43.20	W	C/D	Dark	23 Oct	Mon	1900	0	0
822194	43.77	W	C/D	Day	23 Oct	Mon	0800	0	0
786373	46.21	E	C/D	Day	23 Oct	Mon	1000	0	0
825910	46.21	E	C/D	Day	26 Oct	Thurs	1000	0	0
825911	46.90	W	R/W	Dark	28 Oct	Sat	0500	0	3
853508	46.90	E	R/W	Day	28 Oct	Sat	1200	0	0
822853	47.20	W	C/D	Day	24 Oct	Tues	1400	0	0
822196	52.00	W	C/D	DNDK	23 Oct	Mon	1800	0	0
822218	53.51	S	R/W	Day	28 Oct	Sat	0900	0	0
822248	53.51	S	R/W	Day	28 Oct	Sat	0900	0	1
822845	53.51	E	R/W	DNDK	29 Oct	Sun	1600	0	0
822844	53.51	E	R/W	DNDK	29 Oct	Sun	1600	0	0
825915	53.57	E	C/D	Day	28 Oct	Sat	1100	0	1
825905	54.20	E	C/D	Day	25 Oct	Wed	1300	0	0
806972	55.20	N	R/W	Day	28 Oct	Sat	1200	0	0
822198	57.40	E	C/D	Dark	23 Oct	Mon	1900	0	0
822199	57.80	W	C/D	Day	24 Oct	Tues	0800	0	0
825917	58.48	W	R/W	Day	28 Oct	Sat	1000	0	0
825920	58.92	E	C/D	Day	29 Oct	Sun	1500	0	0
792851	59.45	E	C/D	Day	23 Oct	Mon	1200	0	0
803870	60.03	S	C/D	Dark	29 Oct	Sun	1900	0	0